Whole-rock and zircon evidence for evolution of the Late Jurassic high Sr/Y Zhoujiapuzi granite, Liaodong Peninsula, North China Craton

Renyu Zeng [a, b,c] *, Mark B. Allen [c], Xiancheng Mao [d], Jianqing Lai [d], Jie Yan [a, b], Jianjun Wan[a, b]

[a] State Key Laboratory of Nuclear Resources and Environment, East China University of Technology, Nanchang, 330013, Jiangxi, China

[b] School of Earth Sciences, East China University of Technology, Nanchang, 330013, China

[c] Department of Earth Sciences, Durham University, Durham DH1 3LE, UK

[d] School of Geosciences and Info-Physics, Central South University, Changsha 410083, China

Correspondence: Renyu Zeng (zengrenyu@126.com)

Abstract: Middle-Late Jurassic high Sr/Y granitic intrusions are extensively exposed in the Liaodong Peninsula, in the eastern part of the North China Craton (NCC). However, the genesis of the high Sr/Y signature in these intrusions has not been studied in detail. In this study, we report results of zircon U-Pb dating, Hf isotopic analysis and zircon and whole-rock geochemical data for the Late Jurassic Zhoujiapuzi granite in the middle part of the Liaodong Peninsula. The Zhoujiapuzi granite is high-K (calc-alkaline) and peraluminous in nature, with high SiO_2 (68.1–73.0 wt %) and Al_2O_3

(14.5–16.8 wt %), low in TFe_2O_3 (1.10–2.49 wt %) and MgO (0.10–0.44 wt %), and with high Sr/Y (19.9–102.0) and La_N/Yb_N (14.59–80.40), characteristic of high Sr/Y I-type granite. The geochemical signatures, in combination with the presence of a large number of Paleoproterozoic inherited zircons, indicate that the Zhoujiapuzi granite was most likely derived from partial melting of the basement in the region, and specifically the Liaoji granites. The high Sr/Y signature is inherited from these source rocks. LA-ICP-MS zircon U-Pb dating of the autocryst zircons from two samples (from different localities) yielded consistent weighted average ages of 160.7±1.1 Ma (MSWD=1.3) and 159.6±1.1 Ma (MSWD=1.2), with εHf(t) values in the range of -26.6– -22.8. Morphological and chemical studies on autocrystic zircon grains show that there are two stages of zircon growth, interpreted as magmatic evolution in two distinct stages. The light-CL core reflects a crystallization environment of low oxygen fugacity and high $T_{Zr\text{-}Ti}$; the dark-CL rim formed with high oxygen fugacity and lower $T_{Zr\text{-}Ti}$. Based on the geochemical features and regional geological data, we propose that the Liaodong Peninsula in the Late Jurassic was part of a mature continental arc, with extensive melting of thick crust above the Paleo-Pacific subduction zone.

Keywords: Liaodong Peninsula; Late Jurassic; Zircon U-Pb-Hf isotopes; Two stages of crystal growth; High Sr/Y granite

1. Introduction

The Liaodong Peninsula is located in the northeast of the North China Craton (NCC). The northeast NCC was influenced by three main tectonic regimes in the Mesozoic, related to the subduction of the Paleo-Asian, Paleo-Pacific and Mongol-

Okhotsk oceans (Tang et al., 2018). The superposition of these different regimes resulted in changing tectonic and magmatic patterns over time. Middle-Late Jurassic granitic rocks are extensively exposed in the northern parts of the Liaodong Peninsula, such as the Yutun mylonitic granite, Xiaoheishan granodiorite, Heigou monzogranite (Wu et al., 2005), Wulong two-mica monzogranite (Yang et al., 2018), and Huangdi biotite monzogranite (Xue et al., 2020). Most of these rocks are characterized by high Sr /Y, and plot within the adakite field on Sr/Y-Y and La_N/Yb_N-Yb_N diagrams (Wu et al., 2005a; Yang et al., 2015a, 2018).

The geodynamic settings and petrogenesis of adakite and geochemically similar high Sr/Y igneous rocks have been widely discussed. The high Sr/Y rocks were originally proposed to be formed by melting of young (<25 Ma) and hot subducted oceanic slab in an arc setting (Defant and Drummond, 1990). However, later studies have shown that the high Sr/Y rocks can form in both arc and non-arc settings by other processes, such as continental interior settings (Wang et al., 2007), cold subduction zones (Nakamura and Iwamori, 2013), collision or post-collision processes (Schwartz et al., 2011). In addition, numerous studies have suggested that the lower continental crust can also be the source of the high Sr/Y rocks (Gao et al., 2004; Ou et al., 2017). However, it is debated whether crustal thickening is necessary for their formation (e.g. Moyen, 2009; Kamei et al., 2009; Zhan et al., 2020). In recent years, some studies have proposed that the high Sr/Y ratio in granitic rocks can be inherited from a high Sr/Y crust source, regardless of pressure (Kamei et al., 2009; Ma et al., 2015; Zhan et al., 2020).

The Middle-Late Jurassic granitic rocks in the Liaodong Peninsula are commonly proposed to be the products of partial melting of thickened mafic crust with garnet in the residue (Wu et al., 2005a; Yang et al., 2015a, 2018; Tang et al., 2018). However, the

source composition has not been fully considered in the petrogenesis of the high Sr/Y rocks in the Liaodong Peninsula. Hence, the petrogenesis of the Middle-Late Jurassic high Sr/Y rocks needs to be re-evaluated, based on more detailed work and a consideration of possible sources. This petrogenesis is of significance for understanding the Jurassic tectonics of the Liaodong Peninsula, and the NCC in general.

In this paper, we examined the high Sr/Y Zhoujiapuzi granite from the Xiuyan area, in the middle of the Liaodong Peninsula. Zircons are analysed for U-Pb-Hf isotopes and trace element geochemistry, and by Raman spectroscopy. These results are integrated with whole-rock geochemistry. We focus on the zircons, because of their potential to reveal the origins of the pluton (Belousova et al., 2002; Wang et al., 2007; Breiter et al., 2014; Zhao et al., 2014), and so provide a case study for the evolution of plutonic magma systems in general. Based on observations of the CL images and chemical analysis, two zircon growth stages can be distinguished. We first determine the crystallization environments of the two zircon growth stages, and then decipher the petrogenesis, source characteristics and origin of the high Sr/Y signature of the pluton as a whole. Integrated with previous studies, our study provides insights into the tectonic evolution of the Liaodong Peninsula in the Late Jurassic.

2. Geological setting

The Zhoujiapuzi granite is located in the middle of the Liaodong Peninsula, at the northeastern margin of the NCC (Fig. 1). The Paleoproterozoic Liaohe Group and Liaoji granite are the basement in the study area. The Liaohe Group includes the Lieryu, Gaojiayu, Dashiqiao and Gaixian formations. Although stratigraphic terms are used, these rocks are metamorphic, and the group consists of leptynite, leptite, granulite,

amphibolite, marble and phyllite. The protoliths of the Liaohe Group include marine volcanics, clastics, carbonates and claystones. The formation age of the metasedimentary rocks in the Liaohe Group is 2.0–1.9 Ga (Wan et al., 2006; Li et al., 2015). It is in unconformable contact with the overlying strata of the Mesoproterozoic Cuocaogou Formation and Xiaoling Formation.

The study area experienced strong magmatic activity in the Paleoproterozoic, which can be divided into two stages of 2.2–2.1 Ga and ~ 1.85 Ga. The 2.18–2.14 Ga Liaoji granites (also called gneissic granites), which lie within an area measuring 300 km × 70 km, are dominated by A- and I-type granites (Li and Zhao, 2007; Yang et al., 2016; Wang et al., 2020a). Metamorphosed volcanic rocks (leptynite, leptite and granulite) in the Liaohe Group also formed at 2.2–2.1 Ga (Li et al., 2015). The ~1.85 Ga granites mainly consist of I- and S-type porphyry granites and alkaline syenites (Yang et al., 2007; Yang et al., 2015b). In addition, there were small amounts of mafic magmatic activity at ~2.17 Ga, ~2.1 Ga and ~1.8 Ga (Meng et al., 2014; Yuan et al., 2015). There are a variety of viewpoints on the Paleoproterozoic tectono-magmatic evolution in the Liaodong Peninsula, such as an intracontinental rift opening-closing model (Li et al., 2005) and an arc-continent collision model (Faure et al., 2004).

In the Mesozoic, the region of the Liaodong Peninsula was influenced by the circum-Pacific tectonic regime, the Mongol-Okhotsk tectonic regime and the Paleo-Asian Ocean tectonic regime. The joint influence of multiple tectonic regimes resulted in intensive magmatism during the Mesozoic (Fig. 1b). These Mesozoic magmatic rocks can be divided into three stages, namely: Triassic (233–212 Ma), Jurassic (180–

115 156 Ma) and Early Cretaceous (131–117 Ma) (Wu et al., 2005b).

116 The Triassic magmatic rocks are less exposed, mainly alkaline rocks, diabase,
117 diorites and granites (Wu et al., 2005b). Among them, the granites mainly have A-type
118 affinity, and may have formed in an extensional setting (Tang et al., 2018; Wang et al.,
119 2019). Magmatism has been related to either the subduction of the Paleo-Pacific slab,
120 closure of the Paleo-Asian Ocean, or the collision between the NCC and the Yangtze
121 Craton (Tang et al., 2018; Wang et al., 2019). The majority of the Jurassic magmatic
122 rocks are monzogranite and granodiorite, which are generally calc-alkaline I-type
123 granites, and show characteristics of adakite-like rocks. Some of them, exposed near
124 later extensional structures, have undergone regional ductile deformation. These
125 Jurassic magmatic rocks are generally considered to relate to the subduction of the
126 Paleo-Pacific slab (Wu et al., 2005a; Zhai et al., 2004). In the Early Cretaceous, basic-
127 acidic-alkaline rocks were widely developed. Among them, the granites have mainly
128 A- and I-type affinities. These rocks are generally considered to have formed in an
129 intense extensional environment, which is connected with either the rollback or low-
130 angle subduction of the Paleo-Pacific slab (Wu et al., 2005c; Zheng et al., 2018).

131 **3. Samples and petrography**

132 The Zhoujiapuzi granite is located to the east of Xiuyan City, in the middle of the
133 Liaodong Peninsula (Fig. 1b). It intruded into the Lieryu Formation of the Liaohe Group.
134 Eight samples of the Zhoujiapuzi granite were collected at locations shown in Fig. 1c.

135 The Zhoujiapuzi granite is generally grey in colour and with fine-grained texture

(Fig. 2a). The mineral assemblage contains K-feldspar (~50 %), quartz (~25 %), plagioclase (~20 %) and biotite (~5 %) as well as accessory minerals such as zircon, ilmenite, magnetite and apatite. K-feldspar grains are euhedral or subhedral, and always exhibit cross-hatched twinning (Fig. 2b). Quartz grains are usually xenomorphic, and have indented boundaries and wavy extinction (Fig. 2b-d). Plagioclase always exhibits polysynthetic twinning and have sericitization in places (Fig. 2c). Biotite mainly fills in the interstices between the other minerals (Fig. 2c, d).

4. Analytical methods

The cathodoluminescence (CL) images of zircon were obtained by the Chengpu geological Testing Co. Ltd, Langfang, China using the TIMA analysis. The LA-ICP-MS zircon U-Pb analyses were performedusing an Agilent Technologies 7700x ICP-MS with a Teledyne Cetac Technologies Analyte Excite laser-ablation system at Nanjing FocuMS Contract Testing Co. Ltd. The analyses were carried out with a 35 μm spot size at 8 Hz repetition rate for 40 seconds. The ICP-MS detector has dual modes: pulse for lower signal, and analog for higher signal. Pulse-analog cross calibration was performed before the measurement of U-Pb isotopes, delivering a wider linear dynamic range – up to 10 orders of magnitude. For a signal of ^{238}U higher than 1.2–1.4 Mio cps, equivalent zircon contains U concentrations higher than 600 ppm, and are measured in analog mode. 91500 was used as external standard. GJ-1 (600Ma, Jackson et al., 2004) and Plešovice (337Ma, Sláma et al., 2008) were treated as quality control for geochronology. During our analyses, the weighted mean age of GJ-1 and Plešovice were 606.0 ± 4.8 Ma (n=16, MSWD = 0.50) and 340.9 ± 4.0 Ma (n=7, MSWD = 1.0), respectively. Trace elements abundance of zircon were externally calibrated against

NIST SRM 610 with Si as the internal standard. The raw ICP-MS data were processed using ICPMSDataCal software (Liu et al., 2010). No common-Pb correction was applied to the data. Data reduction was completed using the Isoplot4.15 (Ludwig, 2003). The instrument description and analytical procedure are described in detail by Zeng et al. (2018).

The in-situ Lu-Hf isotopic analyses of zircon were performed by LA-MC-ICP-MS using a Teledyne Cetac laser-ablation system and a Nu Plasma II MC-ICP-MS at Nanjing FocuMS Contract Testing Co. Ltd. The 193 nm ArF excimer laser was focused on zircon surface with fluence of 6.0J/cm^2. The ablation protocol employed a spot diameter of 50 um at 8 Hz repetition rate for 40 seconds. Three standard zircons, GJ-1, 91500, and Penglai, were analysed for quality control at every ten unknown samples. In the experiment, standard zircon GJ-1, 91500, and Penglai were analyzed, and the $^{176}Hf/^{177}Hf$ ratios were 0.282002–0.282013, 0.282305–0.282315 and 0.282901–0.282914 respectively, in accordance with their recommended values (GJ-1: 0.282012, Yuan et al., 2008; 91500: 0.282307 ± 0.000031, Wu et al., 2006; Penglai: 0.282906 ± 0.000010, Li et al., 2010). For the calculation of εHf(t) values, we have adopted the ^{176}Lu decay constant of 1.867×10^{-11} (Söderlund et al., 2004), the present-day chondritic values of $^{176}Lu/^{177}Hf = 0.0332$ and $^{176}Hf/^{177}Hf = 0.282772$ (Blichert-Toft and Albarède 1997). To calculate one-stage model ages (T_{DM1}) relative to a depleted-mantle source, we have adopted the present-day depleted-mantle values of $^{176}Lu/^{177}Hf = 0.0384$ and $^{176}Hf/^{177}Hf = 0.28325$ (Vervoort and Blichert-Toft 1999). To calculate two-stage modal ages (TDM2), 'felsic crust' model ages are calculated using average continental crust $^{176}Lu/^{177}Hf = 0.015$ (Griffin et al., 2004)

Zircon Raman analyses were carried out using an RM2000 laser Raman spectrometer at the State Key Laboratory of Nuclear Resources and Environment, East China University of Technology. The selected incident wavelengths were 532 and 785 nm in order to clearly identify the luminescence bands due to low concentration impurities. The beam power was 20 mW. The Leica 50× objective was employed.

Six fresh rock samples were selected for geochemical analysis. The elemental analyses were conducted at Analytical Chemistry & Testing Services (ALS) Chemex (Guangzhou) Ltd. Major oxides were analyzed using wave-dispersive X-ray fluorescence (XRF) (ME-XRF26). Analytical precision was better than ± 0.01%. Trace element abundances were measured by the lithium borate dissolution method and ICP-MS (ME-MS81). The analytical uncertainties of the rare earth element (REE) and high field strength element (HFSE) are <5%. Analytical uncertainties are in the range of 5%–10% for the other elements. Detailed analytical procedures refer to Zhang et al. (2019) and Nash et al. (2020).

5. Analytical results

The data for major and trace elements, Raman microprobe data, zircon trace elements, zircon U-Pb ages, and zircon Hf isotopes are shown in Tables S1, S2, S3, S4 and S5, respectively.

5.1. Whole-rock major and trace element compositions

SiO_2 contents range from 68.11 wt.% to 73.02 wt.% (average 71.71 wt.%). Contents of Na_2O and K_2O are 3.81 – 4.65 wt.% and 4.32 – 4.71 wt.%, respectively,

with Na_2O/K_2O ratio of 0.82 – 1.08 and total alkalis ($Na_2O + K_2O$) of 8.38 – 8.97. All samples plot in the field of granite in the TAS classification except one (Fig. 3a). These samples have Al_2O_3 contents of 14.49 – 16.83 wt.% (average 15.09 wt.%), CaO contents of 1.04 – 1.98 wt.% (average 1.38 wt.%) and A/CNK values of 1.05 – 1.10 (average 1.07). In the A/NK – A/CNK diagram (Fig. 3b), all samples plot in the peraluminous field (Fig. 3b). The granite samples have low TFe_2O_3 (TFe_2O_3 = all Fe calculated as Fe_2O_3) contents and MgO contents ranging from 1.10–2.49 wt % and 0.10–0.44 wt %, respectively, with Mg# (Mg#=100*molar Mg/(Mg+Fe)) values of 15–26.

The samples of the Zhoujiapuzi granite exhibit variable REEs, with total REEs ranging from 59 to 302 ppm. The La_N/Yb_N values of the Zhoujiapuzi granite range from 14.59 to 80.40 (average 38.27), showing right-declined REE patterns (Fig. 4a). The samples have Eu/Eu* of 0.62–1.94 and Ce/Ce* of 0.94–1.16. In the primitive mantle-normalized trace element diagram (Fig. 4b), the samples show negative anomalies of HFSEs (e.g., Nb, Ta, Ti and P) and positive anomalies of La and LILEs (e.g., K, Rb, Ba, U, La, Ce). The Zhoujiapuzi granite is characterized by high contents of Sr (309–551 ppm) and low contents of Y (5.01–15.5 ppm) and Yb (0.43–1.40 ppm), with high Sr/Y ratios of 19.94–102.04 (average 65.50).

5.2 Zircon CL images, Raman spectra and REE elements

CL images of zircons from the Zhoujiapuzi granite are shown in Fig. 5. Zircons commonly have crystal sizes between 150 and 250 μm, and have length/width ratios of 2:1–4:1, with euhedral, stubby to elongate prisms. According to the CL images, most zircons show an internal division into 2 distinct domains: light-CL core and dark-CL

rim. The light-CL core is characterized by bright CL intensity and widely-spaced oscillatory zoning patterns. The dark-CL rim is overgrown continuously by the light-CL core and is characterized by extremely low CL emission and narrowly-spaced oscillatory zoning patterns. In addition, some zircons have inherited cores, which have corroded and rounded shapes in contact with the light-CL core, such as 1# and 37# in XY-001 and 6# and 41# in XY-008 (Fig. 5). These inherited zircons have oscillatory zoning in CL images.

Six light-CL core spots and six dark-CL rim spots were analyzed for Raman spectra. The light-CL cores have antisymmetric stretching vibration (B_{1g}) of the SiO_4 tetrahedra (v_3 (SiO_4)) Raman band of 1005–1007 cm^{-1} and half-width of the v_3 (SiO_4) Raman band (b) values of 6.0–8.1 cm^{-1}, while the dark-CL rims have v_3 (SiO_4) Raman band of 1004–1007 cm^{-1} and b values of 5.4–9.0 cm^{-1}.

Twenty light-CL core spots, eighteen dark-CL rim spots and six inherited zircon spots were analyzed for trace and rare earth elements. The light-CL core spots have lower U content (28–677 ppm) than the dark-CL rim spots (U=641–3842 ppm). In the chondrite-normalized REE element diagram (Fig. 6a, b), both the light-CL core and dark-CL rim are characterized by HREE enrichment relative to LREE with positive Ce anomalies and negative Eu anomalies. The light-CL core spots have ΣREE of 49–1115 ppm (average 390 ppm), ΣLREE of 3–72 ppm (average 14 ppm) and ΣHREE of 46–1100 ppm (average 377 ppm), whereas the dark-CL rim spots have ΣREE of 327–1632 ppm (average 895 ppm), ΣLREE of 2–14 ppm (average 6 ppm) and ΣHREE of 325–1627 ppm (average 889 ppm). Hence, the REE content of the light-CL core is significantly lower than that of the dark-CL rim, and the difference between the two is mainly in HREE content. The light-CL core spots have Eu/Eu* of 0.07–0.60 (average 0.28) and Ce/Ce* of 1.89–24.27 (average 10.03). Because the contents of La and Pr are

typically present very low, Ce* in this study is obtained by the formulation $(Nd_N)^2/ Sm_N$ (Loader et al., 2017). The dark-CL rim spots have Eu/Eu* of 0.08–0.24 (average 0.13) and Ce/Ce* of 6.57–200.31 (average 79.23). These results indicate that the light-CL core have a weaker negative Eu anomaly and a weaker positive Ce anomaly than those of the dark-CL rim. The inherited zircon spots have ΣREE of 602–1517 ppm, and show depletion of LREE, enrichment of HREE, a positive Ce anomaly (Ce/Ce* of 1.52–216.08) and a negative Eu anomaly (Eu/Eu* of 0.07–0.13) (Fig. 6c).

5.3 Zircon U–Pb and Hf isotope composition

Seventy-seven spots were analysed for U-Pb isotope composition from samples XY-001 and XY-008. In the U-Pb Concordia diagram (Fig. 7a, c), both the light-CL core and dark-CL rim spots overlap within uncertainty on the Concordia curve. There is a large degree of overlap between the 29 spots of dark-CL rim and 32 spots of light-CL core in terms of $^{206}Pb/^{238}U$ age although the average value for $^{206}Pb/^{238}U$ age is higher in the 32 spots of light-CL core (Fig. 7e). On a single zircon, the $^{206}Pb/^{238}U$ age of the light-CL core is older than that of the dark-CL rim (Fig. 5), but the two values are within the error range of the in-situ LA-ICP-MS analyses (individual spot of ±3–5% relative precision, Schmitz and Kuiper, 2013). In sample XY-001, 33 spots define a weighted mean $^{206}Pb/^{238}U$ age of 160.7±1.1 Ma (2σ, MSWD=1.3; Fig. 7b). In sample XY-008, 28 spots define a weighted mean $^{206}Pb/^{238}U$ age of 159.6±1.1 Ma (2σ, MSWD=1.2; Fig. 7d). The other 10 spots with distinctly older ages ($^{207}Pb/^{206}Pb$ ages ranging from 2500 to 2173 Ma) were obtained on inherited cores. Their ages are discordant, suggesting that these inherited cores were variably influenced by lead loss. Among these, 9 spots define a discordia line with an upper intercept age of 2163 ± 13 Ma (MSWD=0.45) (Fig. 7f).

Twenty-four zircons were analyzed for Lu-Hf isotope composition. The variation in Hf isotopic data is limited, between 9 spots from light-CL core and 9 spots from dark-CL rim. 18 spots exhibit a range of $^{176}Hf/^{177}Hf$ ratios from 0.281921 to 0.282030, which converts to εHf(t) values between -26.6 to -22.8 (Fig. 8), and two-stage Hf model (T_{DM2}) ages of 2650 to 2889 Ma by using the U-Pb age for each zircon. Six analytical spots, which define the Concordia upper intercept age of 2163 Ma, show $^{176}Hf/^{177}Hf$ radios and εHf(t) values of 0.281443 to 0.281496 and -0.7 to 1.5, respectively, with T_{DM2} age of 2648 Ma to 2791 Ma by using the upper intercept age.

6. Discussion

6.1 Significance of the two stages of zircon

Generally, zircon with high U content can easily break down into the metamict state because of the radiation damage to the lattice caused by α-particles originating from the decay of uranium (Mezger and Krogstad, 1997). The physical and structural changes often lead to the loss of Pb and addition of trace elements such as LREE. In this study, the dark-CL rim spots have high U content, which is significantly higher than the median value of zircon U content in granitic magma (350 ppm, Wang et al., 2011). Hence, the metamictization degree of the zircons must be taken into consideration. Data from dark-CL rim spots plot on the Concordia curve, indicating no obvious Pb loss. The internal structure of dark-CL rim is relatively intact, with obvious oscillatory zoning, and few cracks, implying that the physical and structural of the dark-CL rim remained unchanged. Nasdala et al. (1998) suggested that the metamictization of zircon can be well characterized by Raman spectroscopy. The half-width of the $v_3(SiO_4)$ Raman band

297 (*b*) of 10 cm^{-1} and 20 cm^{-1} are proposed to approximately distinguish well-crystallized,
298 intermediate and metamict zircons (Nasdala et al., 1998). The dark-CL rim have *b*
299 values of 5.4–9.2, characterizing them as well-crystallized. Therefore, the above
300 features indicate that the dark-CL rim are not metamict. Consequently, it can be
301 concluded that the U-Pb isotope and trace element systematics of the dark-CL rim have
302 not been changed by metamictization.

303 Both the light-CL core and dark-CL rim have oscillatory zoning patterns, and their
304 chondrite-normalized REE patterns are characterized by steeply positive slopes from
305 the LREE to HREE with strong negative Eu anomalies and pronounced positive Ce
306 anomalies. The above characteristics are consistent with those of igneous zircon
307 (Hoskin and Schaltegger, 2003). Although hydrothermal zircon can also have
308 oscillatory zoning patterns similar to magmatic zircons, there are obvious differences
309 in trace elements between the magmatic and hydrothermal zircon (Hoskin et al., 2005).
310 In the discrimination diagram (Fig. 9), both the spots of light-CL core and dark-CL rim
311 fall in or near the magmatic field, which is obviously different from hydrothermal
312 zircon. Hence, the above characteristics indicate that both the light-CL core and dark-
313 CL rim have a magmatic origin.

314 The light-CL core was overgrown continuously by the dark-CL rim. In addition,
315 the contact between the light-CL core and dark-CL rim is euhedral. Such core-mantle
316 overgrowth relationships indicate that the light-CL core domains are not inherited
317 zircons. The similar Hf isotopic data of the light-CL core and dark-CL rim is also
318 consistent with this interpretation. For the age population, the samples of XY-001 and

XY-008 have MSWD of 1.3 and 1.2, respectively, which are both within the expected range for 95 % confidence interval (Mahon, 1996). Although the $^{206}Pb/^{238}U$ age of dark-CL rim is generally younger than that of light-CL core, the ages of these two distinct domains have the characteristics of continuous variation, and do not show two or more distinct age populations (Fig. 7b, d). These phenomena do not support the presence of antecrystic zircons (Siégel et al., 2018). Hence, both the light-CL core and dark-CL rim are most likely autocrystic zircon formed in one distinct pulse of magma. The weighted mean U-Pb ages of 160.7±1.1 Ma and 159.6±1.1 Ma can be interpreted as the emplacement age of the Zhoujiapuzi granite. The obvious difference in internal structure and trace element composition between the light-CL core and dark-CL rim could be due to significant changes in their crystallization environments (Wang et al., 2007).

The Zr/Hf ratio in zircon has a negative correlation with the degree of fractionation in the parent melt (Claiborne et al., 2006). In this study, the Zr/Hf ratios of the dark-CL rim (21–40) are obviously lower than those of the light-CL core (39–56) (Fig. 10a). In addition, incompatible elements such as U and REE will become enriched in the highly evolved magma (Zhao et al., 2014). In this study, the contents of U and REE of dark-CL rim are significantly higher than those of light-CL core (Fig. 10a). Overall, the above features reflect that the dark-CL rim crystallized from a later and more evolved magma.

Watson and Harrison (2005) found that the Ti content of zircon has a strong dependence on temperature (T), and obtained a Ti-in-zircon thermometer ($T_{Zr\text{-}Ti}$). Since

then, Ferry and Watson (2007) suggested that the solubility of Ti in zircon depends not only on T and activity of TiO_2 ($aTiO_2$) but also on the activity of SiO_2 ($aSiO_2$), and revised the $T_{Zr\text{-}Ti}$. We use the $T_{Zr\text{-}Ti}$ from Ferry and Watson (2007) and the recommended values ($aSiO_2$=1, $aTiO_2$ = 0.5) for the activity of SiO_2 and TiO_2 (Schiller and Finger, 2019), due to the presence of ilmenite and quartz in the Zhoujiapuzi granite. The $T_{Zr\text{-}Ti}$ from the light-CL core and dark-CL rim are 684–830 ℃ (average 761 ℃) and 509–712℃ (average 635 ℃), respectively, i.e. the light-CL core formed at higher temperatures than the dark-CL rim. The $T_{Zr\text{-}Ti}$ value shows a significant positive correlation with Zr/Hf (a tracer of fractional crystallisation), and shows continual fractionation and cooling (Fig. 10b). As the light-CL core and dark-CL rim formed in different magmatic evolution stages, it is problematic to use the same $aSiO_2$ and $aTiO_2$ values to calculate both $T_{Zr\text{-}Ti}$ values for both. For ilmenite bearing granites, Schiller and Finger (2019) suggested that the variation of $aTiO_2$ values corresponding to different zircon crystallization stages is small. In addition, Schiller and Finger (2019) showed that the $aSiO_2$ value of the ilmenite-bearing granites at the onset of magmatic zircon crystallization was more than 0.75. Even if the $aSiO_2$ value of the light-CL core is changed from 1.0 to 0.75, the temperature will only drop by about ~27 ℃, which is significantly lower than the 126 ℃ difference between the average $T_{Zr\text{-}Ti}$ value of the light-CL core and dark-CL rim. Therefore, it is certain that the light-CL core formed at higher temperatures than the dark-CL rim, although we cannot calculate the specific temperature difference.

Cerium exists in magmas as both Ce^{3+} and Ce^{4+}. Because the 0.84-Å radius of the

363 Zr^{4+} ion is more closely matched by the Ce^{4+} (0.97-Å radius) than the Ce^{3+} (1.143-Å
364 radius) (all ionic radii are from Shannon, 1976), Ce^{4+} is more compatible in the zircon
365 structure than the Ce^{3+}. Hence, the magnitude of Ce anomaly is a useful tool for
366 evaluating the oxygen fugacity condition of crystallization environment (e.g. Ballard et
367 al., 2002; Trail et al., 2012). Loader et al. (2017) suggested that the Ce/Ce* ratio is
368 likely to be the most robust measure of magma redox conditions, although it is only a
369 semi-quantitative measure. In this study, the Ce/Ce^{*} ratio of the light-CL core and dark-
370 CL rim are 6.30–153.36 (average 32.51) and 21.81–5773.06 (average 787.39),
371 respectively. This result suggests that the dark-CL rim formed in a higher oxygen
372 fugacity environment than the light-CL core. As shown in the Ce/Ce*-Zr/Hf diagram
373 (Fig. 10c), Ce/Ce* has a significant negative correlation with Zr/Hf, showing that the
374 oxygen fugacity condition is increasing with the evolution of magma.

375 The absence of enclaves and disequilibrium textures in the Zhoujiapuzi granite
376 and uniform εHf(t) values of the light-CL core and dark-CL rim do not support magma
377 mixing and wall-rock assimilation. Consequently, the abrupt change between the
378 crystallization environment of the light-CL core and dark-CL rim is not due to the
379 magma mixing or contamination during magma evolution. Therefore, we propose that
380 the light-CL core was formed in a relatively deep magma chamber, which had low
381 oxygen fugacity, low Zr saturation and higher temperature. The low Th, U and REE,
382 and widely-spaced oscillatory zoning patterns indicate a low growth rate of zircon
383 (Hoskin and Schaltegger, 2003; Wang et al., 2011). In contrast, the dark-CL rim was
384 formed during the ascent and/or at the emplacement location of the magma. At this

385 stage, the oxygen fugacity significantly increased, the temperature decreased, and Zr
386 saturation increased due to the crystallization differentiation. In this environment, the
387 crystallization rate of zircon significantly increased, forming the zircons with a higher
388 content of Th, U and REE elements, low CL emission and narrowly-spaced oscillatory
389 zoning patterns.

390 Zircon U-Pb dating is the most commonly used method in geochronology,
391 especially dating the emplacement age of magmatic rocks. A weighted mean age or
392 upper intercept age is usually obtained to represent the emplacement time of a magmatic
393 rock. However, the autocrystic zircons in this study record two different magmatic
394 evolution stages. Previous studies, such as Wang et al. (2007), Zhao et al. (2014) and
395 Chen et al. (2020), also show that zircons can crystallize continually or intermittently
396 in a single phase of magmatism, showing several growth zones of clearly different
397 internal structure and distinct time difference. Therefore, autocrystic zircon can be
398 formed in two or more evolution stages during one distinct pulse or increment of
399 magma. Some scholars even regard that the age difference of different stages can be
400 more than dozens of Ma (Wang et al., 2007). Therefore, if the zircon ages in the same
401 magmatic rock have a large range of variation, this could be caused by the zircons
402 recording different stages in magmatic evolution, related to different levels of magma
403 within the crust and/or different temperature regimes. In this paper, although the
404 apparent age of the dark-CL rim is generally younger than that of the light-CL core, the
405 age difference between the two is within the error range of the in-situ LA-ICP-MS
406 analyses (individual spot of ±3–5% relative precision). Therefore, further work is

needed to verify the actual age difference between the two magmatic evolution stages. Nevertheless, it is notable that the bulk petrology and geochemistry of the host pluton does not record and reveal this two-stage magmatic evolution, which can only be detected in the zircon analysis.

6.2 Genetic type: I-type affinity

The Zhoujiapuzi granite has low Zr (113 – 242 ppm), Ce (26.5 – 121.5 ppm), Zr+Nb+Ce+Y (152.0 – 382.6 ppm), $(Na_2O + K_2O)/CaO$ (4.53 – 8.31) and FeO*/MgO (5.09 – 10.56), distinct from the typical A-type granites (Fig. 11a-d). Furthermore, the Zhoujiapuzi granite does not contain mafic alkaline minerals, such as arfvedsonite, riebeckite, etc., which is also distinctly inconsistent with typical A-type granites (Wu et al., 2003). Wu et al. (2017) suggested that a high formation temperature is one of the most important characteristics of A-type granite. Zircon saturation thermometry (T_{Zrn}) and Ti-in-zircon thermometer ($T_{Zr\text{-}Ti}$) are two methods for estimating magma temperatures. As noted above, because the values of $aSiO_2$ and $aTiO_2$ during the early zircon crystallization cannot be accurately obtained, the temperature of this period cannot be accurately obtained through the Ti-in-zircon thermometer. Zircon saturation thermometry was introduced by Watson and Harrison (1983) and is suitable for non-peralkaline crustal source rocks. Since the zircon solubility is mainly affected by temperature, major element compositions have a limited impact on calculated T_{Zrn} (Miller et al., 2003). In addition, the errors introduced by crystal-rich composition tend to cancel as changes in Zr concentration and M value during crystallization have

opposite effects on the T_{zrn} value (Miller et al., 2003). Therefore, the composition of Zhoujiapuzi granite can be used to estimate the magma temperature. The calculated T_{Zrn} values for the Zhoujiapuzi granite are in the range of 803-870 °C (mean=845 ±20°C). It was proposed that the T_{Zrn} suggests an upper limit on the temperature of melt generation for inheritance-rich granitoid (Miller et al., 2003). Hence, the magma temperature of the Zhoujiapuzi granite should be lower than or equal to the T_{Zrn} value, which is significantly lower than that of typical A-type granite (>900 ℃, Skjerlie and Johnston, 1992; Douce, 1997). Thus, the Zhoujiapuzi granite is not an A-type granite.

The samples of the Zhoujiapuzi granite have A/KNC < 1.1, relatively high Na_2O (3.96–4.65 wt.%) and lack peraluminous minerals (e.g. cordierite, andalusite, muscovite and garnet), which are clearly different from S-type granites (Chappell and White, 1992). With the rise of the degree of crystallization, P_2O_5 contents (generally>0.1 wt.%) increase in S-type granites, accompanied by an increase/immutability in SiO_2 (Wolf and London, 1994). However, the Zhoujiapuzi granite samples have low P_2O_5 contents (0.02 – 0.08 wt.%), and decrease with increasing SiO_2 (Fig. 11e), which are features consistent with the I-type granite rather than S-type granite (Chappell and White, 1992). Additionally, Rb has a positive correlation with Y (Fig. 11f), which has been considered as an indicator of I-type granite (Jiang et al., 2018). Furthermore, the composition of the Zhoujiapuzi granite fall in the I-type granite field in the discrimination diagrams of granites introduced by Collins et al. (1982) (Fig. 11 c-d). Therefore, we conclude that the Zhoujiapuzi granite is a I-type granite.

6.3 Petrogenesis of the high Sr/Y granite

The samples of the Zhoujiapuzi granite have high Sr/Y and $(La/Yb)_N$ ratios and low Y and Yb contents (Fig. 12a) consistent with the geochemical signatures of modern adakites (Defant and Drummond, 1990). However, other geochemical parameters of the Zhoujiapuzi granite, such as the high K_2O/Na_2O ratio (0.93 –1.22), low Al_2O_3 content (14.49 –15.02%, except one) and Sr content (in half of the samples lower than 400 ppm), are obviously different from typical adakites ($K_2O/Na_2O \leqslant 0.42$, $Al_2O_3 \geqslant$ 15 %, Sr>400 ppm, Defant and Drummond., 1990; Drummond et al., 1996, Martin et al., 2005). A variety of petrogenetic models have been proposed for the origin of high Sr/Y magmatic rocks, such as partial melting of subducting oceanic crust (Model A, Defant and Drummond, 1990), delaminated lower continental crust (LCC) (Model B, Kay and Kay, 1993; Xu et al., 2002), differentiation of basaltic arc magma (Model C, Castillo et al., 1999), magma mixing between mantle-derived mafic and crust-derived silicic magmas (Model D, Ma et al., 2013a), partial melting of thickened basaltic LCC (Model E, Gao et al., 2004; Ou et al., 2017), or melting of a high Sr/Y (and La/Yb) source (Model F, Kamei et al., 2009; Ma et al., 2015).

6.3.1 Model A: Partial melting of subducting oceanic crust

The partial melting of the young, hot and hydrated subducted oceanic slab in the garnet stability field is the classical formation model of adakite (high Sr/Y rock) (Defant and Drummond, 1990). Studies have shown that the rock with this genetic model generally has the characteristics of high mantle components (such as MgO, CaO and Cr) because of the involvement of mantle magma (Wang et al., 2018). However, this phenomenon was not seen in the Zhoujiapuzi granite. In addition, the Zhoujiapuzi granite has high K_2O/Na_2O ratios (0.92–1.22, average 1.13), which is inconsistent with

474 the slab-derived adakites (K_2O/Na_2O= ~0.4, Martin et al., 2005). Moreover, the low
475 εHf(t) values (-26.6 to -22.8) of the Zhoujiapuzi granite are also inconsistent with the
476 magmas derived from the partial melting of oceanic crust, which generally have
477 depleted isotopic character (Zhan et al., 2020). Furthermore, the Zhoujiapuzi granite
478 has low Ti/Eu and high Nd/Sm radios (Fig. 13a), and markedly negative Nb-Ta
479 anomalies (Fig. 4b), which are distinct from those of oceanic basalts (Yu et al., 2012).
480 In summary, the Zhoujiapuzi granite is difficult to explain by Model A.

481 **6.3.2 Model B: Delaminated lower continental crust (LCC)**

482 High-density, garnet-bearing mafic lower crust delaminating or foundering into
483 the asthenosphere mantle and subsequent interaction with mantle peridotite could
484 produce high Sr/Y magmas (Kay and Kay 1993). Because the melt formed by partial
485 melting of the delaminated lower crust would interact with mantle peridotite during
486 magma ascent, the high Sr/Y magmas related to this petrogenetic model generally have
487 high MgO, Mg# and TiO_2 (Gao et al., 2004; Ou et al., 2017; He et al., 2021). The MgO
488 (0.10– 0.44 wt.%), Mg# (15– 26) and TiO_2 (0.09– 0.34 wt.%) values of Zhoujiapuzi
489 granite are significantly lower than the above values (Fig. 13b- d). In addition,
490 delamination of the lower crust generally occurs in within-plate extensional settings
491 (Gao et al., 2004), and will form a large number of Mg-rich (Mg#>50) rocks due to the
492 partial melting of lithospheric mantle and/or upwelling of asthenosphere (Ou et al.,
493 2017). However, these Jurassic magmatic rocks in the Liaodong Peninsula are generally
494 considered to be formed in a compressional environment related to the subduction of
495 the Paleo-Pacific slab (Li et al., 2004; Yang et al., 2015a; Zhu and Xu, 2019; Zheng et
496 al., 2018). Furthermore, the middle-late Jurassic granites are generally Mg-poor (Fig.
497 13c). Due to the high temperature of the asthenosphere (1200 ℃, Parsons and

McKenzie, 1978; King et al., 2015), rocks formed by partial melting of the delaminated lower crust should possess a high-temperature fingerprint. T_{Zrn} has been used as a geothermometer to estimate partial melting temperatures (e.g., Miller et al., 2003; Collins et al., 2016). As mentioned before, the T_{Zrn} of the Zhoujiapuzi granite is below 900 ℃, which is markedly lower than the temperature of the asthenosphere. Therefore, the petrogenetic model of delaminated lower continental crust (Model B) is also inconsistent with the Zhoujiapuzi granite.

6.3.3 Model C: Differentiation of basaltic arc magma

Low-pressure fractional crystallization (involving olivine + clinopyroxene + plagioclase + amphibole+ titanomagnetite) or high-pressure fractional crystallization (involving garnet) from basaltic magmas have been proposed as two ways to generate adakitic characteristics (Castillo et al., 1999; Macpherson et al., 2006).

However, the composition of the Zhoujiapuzi granite is relatively uniform, including SiO_2, MgO and Na_2O, which does not support major fractional crystallization (Xue et a., 2017). Furthermore, the Zhoujiapuzi granite has abundant inherited zircons and no obvious depletion of Sr, Eu and Ba, showing that this granite has not experienced extensive fractionation (Miller et al., 2003). The samples form clear partial melting trends on the La/Yb versus La diagram (Fig. 13e), which also suggests that partial melting was more important than fractional crystallization (Gao et al., 2007; Shahbazi et al., 2021). In addition, crystal fractionation of basaltic melts can only form minor volumes of granitic melts, the ratio of the two is about 9:1 (Zeng et al., 2016). However, for the same age interval, no coexisting mafic-intermediate rocks have been found in the research area. In the wider region of the Liaodong Peninsula, Middle-Late Jurassic magmatism is dominated by felsic compositions; mafic- intermediate rocks are only

reported in the Huaziyu area (lamprophyre dikes, Jiang et al., 2005). Therefore, it is unlikely that there are large-scale mafic- intermediate rocks contemporaneous with the Zhoujiapuzi granite at depth according to the rock assemblage of Liaodong Peninsula in this period. Moreover, the zircon Hf isotopic compositions of the Zhoujiapuzi granite are quite different from those of the depleted mantle, but are similar to those of the basement (Liaohe Group and Liaoji granite) in the study area (Fig. 8). The ancient inherited zircons (2500 to 2173) with low εHf(t) values also indicate older crustal material in the Zhoujiapuzi granite. For these reasons, it is highly improbable that Zhoujiapuzi granite was derived by differentiation of basaltic magma (Model C).

6.3.4 Model D: Magma mixing between mantle-derived mafic and crust-derived silicic magmas

The Zhoujiapuzi granite has high K_2O/Na_2O ratio (>1) and A/CNK value (>1), together with the absence of mingling textures, mafic microgranular enclaves (MMEs), felsic xenocrysts and melting texture of plagioclase, implying that the mantle-derived magma is unlikely to have played an important role in the genesis of the Zhoujiapuzi granite (Castro et al., 1991). In addition, the Zhoujiapuzi granite is characterized by the development of biotite, but lacks amphibole and pyroxene. These features, coupled with the high A/CNK value, are consistent with an origin as a crust-derived granitoid, but obviously different from the granitoids formed by crust-mantle-derived magma mixing (Barbarin, 1990). Moreover, granites formed by magma mixing generally have high MgO, TFe_2O_3, CaO and Cr contents and low SiO_2 content (Ma et al., 2013a; Wang et al., 2018). These features are obviously inconsistent with the Zhoujiapuzi granite in this study. Additionally, the εHf(t) values and trace element composition of the two stages of zircon also do not support magma mixing. Hence, magma mixing of mantle-derived

546 and crust-derived magmas (Model D) is also unlikely to have produced the Zhoujiapuzi
547 granite.

548 **6.3.5 Model E: Partial melting of thickened basaltic LCC**

549 Experimental studies have shown that the partial melt of basaltic LCC in the garnet
550 stabilization zone (> 40 km, i.e. ~1.2 GPa) can produce magma with a high Sr/Y ratio
551 (Rapp et al., 2003 and references therein). In these scenarios, high Sr/Y and overall
552 adakitic affinity are caused by leaving garnet as residual phases (e.g. Gao et al., 2004).
553 Based on geochemical data for the Zhoujiapuzi granites, partial melting of thickened
554 basaltic LCC is also unlikely to account for the high Sr/Y Zhoujiapuzi granite (Model
555 E). This conclusion is based on the following observations:

556 (1) This ratio of $(Gd/Yb)_N$ is the most important feature to judge whether garnet is
557 involvement in magma genesis (Ma et al., 2012). If the $(Gd/Yb)_N$ ratio of the source is
558 similar to the average value of the LCC (1.71, Rudnick and Gao, 2003), partial melting
559 of these crustal materials controlled by garnet at high pressure can produce melt with
560 $(Gd/Yb)_N$ of 5.8 (Huang and He, 2010). In contrast, the $(Gd/Yb)_N$ values (1.22–5.06,
561 average 2.69) of the Zhoujiapuzi granite are relatively low. (2) Studies of lower-crustal
562 xenoliths show that garnet may not be a common mineral in the lower crust of the NCC
563 (Ma et al., 2012). (3) As shown in the discrimination diagrams of granite sources (Fig.
564 13f, g), all samples fall in the range of metagreywacke-derived melts. Therefore, the
565 Zhoujiapuzi granite was considered to have been derived from crustal anatexis of
566 metagraywacke (or intermediate-acid igneous rock with similar mineral composition),
567 rather than basaltic lower crust.

6.3.6 Model F: Melting of a high Sr/Y (and La/Yb) source

Studies have shown that when a source rock has a high Sr/Y ratio, the high Sr/Y signature of the derived magma can inherit from their source, regardless of pressure (Kamei et al., 2009; Moyen, 2009; Ma et al., 2015). We suggest that partial melting of high Sr/Y Liaoji granite was most probably the origin of the high Sr/Y Zhoujiapuzi granite, as discussed below (Model F).

The Zhoujiapuzi granite has similar mineral assemblages (contains abundant K-feldspar and lacks hornblende) and geochemical composition (Fig. 13h) to the Tsutsugatake intrusion, which is explained by partial melting of arc-type tonalite or adakitic granodiorite (Kamei et al., 2009). Among the inherited zircons from Zhoujiapuzi granite, the ^{207}Pb / ^{206}Pb ages of all the spots are between 2132 and 2200 Ma, except one, and yield a Concordia upper intercept age of 2163 Ma. Both assimilation of country-rocks and incomplete melting of source rocks can explain the genesis of inherited zircon in granite. Due to the similar T_{DM2} of autocrystic zircons (light-CL core and dark-CL rim) and inherited zircons, these inherited zircons most likely come from the source of the Zhoujiapuzi granite. In the study area, meta-sedimentary rocks and meta-volcanic rocks of the South Liaohe Group, Paleoproterozoic mafic rocks, as well as the Liaoji granites, have ~2.16 Ga zircon. In spite of an age peak of 2.17–2.16 Ga in detrital zircon age spectra of the metasediments from the South Liaohe Group, melting of a sediment-dominated source is unlikely to have occurred, as it would have also introduced other age peaks such as ~2.03 Ga and ~2.50 Ga (Li et al., 2015; Wang et al., 2020b). In addition, given the I-type characteristics of the Zhoujipuzi granite, derivation from an igneous precursor is more plausible rather than a metasedimentary origin (Chappell and White, 1992). Therefore, these ~2.16 Ga zircons from the Zhoujiapuzi granite are unlikely to come from the

South Liaohe Group. As shown in the host rock discrimination diagrams (Fig. 14, introduced by Belousova et al., 2002), all the ~2.16 Ga inherited zircons from Zhoujiapuzi granite fall into the granitoid area (Fig. 14), precluding that these ~2.16 Ga zircon come from the Paleoproterozoic mafic rocks. In addition, the ~2.16 Ga inherited zircons from Zhoujiapuzi granite and the zircons from the Liaoji granites lie in a similar area in the εHf(t)-age (Ma) diagram (Fig. 8). Hence, the ~2.16 Ga inherited zircon most likely come from the Liaoji granites.

Some of the Liaoji granites, such as the Muniuhe granite (comprising granodiorite and syenogranite with no distinct boundary between the two), have adakitic signatures, and similar REE and trace element patterns as the Zhoujiapuzi granite (Fig. 4). Based on a model of batch melting (Shaw, 1970) using the experiments of Conrad et al. (1988), the high Sr/Y characteristic of the Zhoujiapuzi granite can be explained by partial melting of Muniuhe granitic pluton leaving amphibole as the main residue (Fig. 12b).

In our modelling, we choose the XY-005 sample to approximately represent the primitive melt composition. The reasons are as below: as mentioned above, the high Sr/Y characteristics of the Zhoujiapuzi granite are not caused by the fractional crystallization of amphibole. Furthermore, the lack of positive correlation between Dy_N/Yb_N ratios and La_N/Yb_N ratios (Fig. 13i) also suggests that fractional crystallization of amphibole was not a significant process for the Zhoujiapuzi granite. On the other hand, the samples of Zhoujiapuzi granite display variable Eu and Sr contents, implying that plagioclase is likely a fractional phase. The separation of titanomagnetite could explain the positive trend in TFe_2O_3 with increasing TiO_2 content, consistent with the occurrences of magnetite in some studied rocks. This possible mineral assemblage of fractional crystallization is also reflected by the chemical variations in the Sr/Y-Y diagram (Fig. 12b). Hence, the sample XY-005, which has

618 highest Sr/Y, was chosen to represent a primitive melt composition. To find the best
619 matching experimental melts, we have compared the major elements of the XY-005
620 sample with that of experimental melts and the characteristics of no garnet residue
621 discussed above. Results are shown in Fig. 12b. The Sr and Y compositions of the
622 starting material used in these experiments resemble those of the average composition
623 of the Muniuhe granitic pluton (Sr=475 ppm, Y=9.77 ppm), if the residue contains a
624 large volume of amphibole (>90 %). However, if more plagioclase is retained in the
625 residue (e.g. 18.3 %), a source region with a higher Sr content is required. Therefore, a
626 similar high Sr/Y Liaoji granite to the Muniuhe granitic pluton can produce the high
627 Sr/Y signatures of the Zhoujiapuzi granite.

628 A large number of Yanshanian adakites (or high Sr/Y rocks) are developed in the
629 NCC, which are generally considered to be derived from the thickened basaltic LCC
630 (e.g. Gao et al., 2004; Wu et al., 2005a; Ma et al., 2013b). Zhang et al. (2001, 2003)
631 suggested that these so-called “C-type adakites” indicated a large-scale crustal
632 thickening event. However, according to the studies on the Triassic and Jurassic adakitic
633 rocks near the Pingquan area, the northern part of the NCC, Ma et al. (2012, 2015)
634 suggested that the adakitic signatures of these rocks are inherited from their source
635 rocks. The research of the Zhoujiapuzi granite in this study also shows that among the
636 widely distributed Jurassic high Sr/Y granites in the Liaodong Peninsula, there is at
637 least one pluton with a high Sr/Y signature inherited from the source. Therefore, we
638 suggest that melting of a high Sr/Y (and La/Yb) source is one of the important processes
639 for the generation of Yanshanian high Sr/Y rocks in the NCC. This kind of high Sr/Y
640 granite does not need to be formed in the garnet stability field.

6.4 Tectonic implications

A large number of Early Jurassic arc-like igneous rocks occur in the northeast part of NCC- Korean Peninsula-Hida belt, which belong to the middle-high K calc-alkaline series and are characterized by enrichment in LILE and depletions in HFSE (Wu et al., 2007; Tang et al., 2018 and references therein). In addition, the Early Jurassic accretionary complexes in the eastern margin of the Eurasian continent and the Japan islands, such as the Heilongjiang complex, the Khabarovsk complex and the Mino-Tamba complex, are considered to be related to subduction (Wu et al., 2007; Tang et al., 2018 and references therein). It is generally accepted that the Paleo-Pacific slab subducted westwards in the Early Jurassic (Tang et al., 2018; Zhu and Xu, 2018).

In the middle-late Jurassic, I-type granites are dominant in the Liaodong Peninsula, such as the Zhoujiapuzi granite (this study), Heigou pluton, Gaoliduntai pluton (Wu et al., 2005a), Waling granite (Yang et al., 2015a) and Wulong granite (Yang et al., 2018). There are not A-type granites, and mantle derived magmatism is extremely rare. These granites were formed by partial melting of crustal materials without obvious contribution of mantle derived magma (Wu et al., 2005a; Yang et al., 2015b, 2018; Xue et al., 2020). In addition, WNW-ESE compression during 157-143 Ma was widespread in the Liaodong Peninsula (Yang et al., 2004; Zhang et al., 2020). It not only mylonitized the granite plutons in middle-lower crust levels, but also intensely deformed the thick sedimentary cover in the upper crust (Qiu et al., 2018; Ren et al., 2020). Hence, Late Jurassic magmatism in the Liaodong peninsula is most likely to be related to subduction of the Paleo-Pacific plate in a mature continental arc, with crust

663 previously thickened by compressional tectonics, related to both the oceanic subduction
664 and the earlier Mesozoic collisions at the north and south margins of the NCC. This
665 setting would produce the conditions required for extensive crustal melting of pre-
666 existing basement. There is a potential resemblance to the modern arc of the Central
667 Andes (Allmendinger et al., 1997), where crustal thickening and plateau growth has
668 developed over the Cenozoic (Scott et al., 2018), and melting of older basement has
669 taken place during subduction of the Nazca plate (Miller and Harris, 1989). This model
670 is also consistent with the idea that much of eastern China was a high orogenic plateau
671 during the Mesozoic, before widespread Early Cretaceous extension and core complex
672 development (Meng, 2003; Chu et al., 2020).

673 **7. Conclusions**

674 (1) LA-ICP-MS zircon U-Pb dating indicates that the Zhoujiapuzi granite in the
675 Liaodong Peninsula formed at ~160 Ma.

676 (2) Zircon growth in Zhoujiapuzi granite can be divided into two distinct stages.
677 The light-CL core was formed in a deeper, hotter, magma chamber, which had low
678 oxygen fugacity and high temperature. The dark-CL rim formed from later, more
679 evolved, magma. Oxygen fugacity significantly increased and the temperature
680 decreased at this stage. The Zhoujiapuzi granite is a case study of multistage generation
681 and emplacement of magma, revealed by zircons, where no signals are discernible in
682 the bulk petrology or geochemistry.

683 (3) The I-type Zhoujiapuzi granite originated from partial melting of the

Paleoproterozoic Liaoji granites. The high Sr/Y compositions are inherited from their source rocks, rather than being a direct indication of deep crustal melting, or any other common mechanism for generating adakitic signatures.

(4) The Late Jurassic tectonic setting of the Liaodong Peninsula and the eastern NCC resembled the modern orogenic plateau of the Central Andes, where silicic magmatism may occur by partial melting of older continental crust in a compressional environment, related to the subduction of the Paleo-Pacific plate.

Acknowledgements

We thank Dr. Wenzhou Xiao, Dr. Jiajie Chen and Dr. Quan Ou for constructive reviews and useful suggestions. We are also grateful to Ying Liu, Chunying Guo, Jianxiong Hu, Ziming Hu for their help with the field work. This research was funded by the National Nature Science Foundation of China (Grants No. 42030809, 41772349, 41902075, 42002095; 42162013), China Scholarship Council (No. 202008360018), Geological Exploration Program of China Nuclear Geology (Grant No. D1802), the research grants from the East China University of Technology (Grant No. DHBK2017103), Open Research Fund Program of State Key Laboratory of Nuclear Resources and Environment (East China University of Technology) (Grant 2020NRE13).

References

Allmendinger, R. W., Jordan, T. E., Kay, S. M., and Isacks, B. L.: The evolution of the Altiplano-Puna plateau of the Central Andes, Annu. Rev. Earth Pl. Sc., 25, 139–174, https://doi.org/10.1146/annurev.earth.25.1.139, 1997.

Altherr, R., Holl, A., Hegner, E., Langer, C. and Kreuzer, H.: High-potassium, calc-alkaline I-type plutonism in the European Variscides: northern Vosges (France) and northern Schwarzwald (Germany), Lithos, 50(1-3), 51–73, https://doi.org/10.1016/S0024-4937(99)00052-3, 2000.

Ballard, J. R., Palin, M. J., and Campbell, I. H.: Relative oxidation states of magmas inferred from Ce(IV)/Ce(III) in zircon: application to porphyry copper deposits of northern Chile. Contrib. Mineral. Petrol., 144, 347–364, https://doi.org/10.1007/s00410-002-0402-5, 2002.

Barbarin, B.: Granitoids: main petrogenetic classifification in relation to origin and tectonic setting, Geol. J., 25, 227–238, 1990.

Belousova, E., Griffin, W., O'Reilly, S. Y., and Fisher, N.: Igneous zircon: trace element composition as an indicator of source rock type, Contrib. Mineral. Petrol., 143, 602–622, https://doi.org/10.1007/s00410-002-0364-7, 2002.

Blichert-Toft, J., and Albarède, F.: The Lu-Hf isotope geochemistry of chondrites and the evolution of the mantle-crust system, Earth. Planet. Sc. Lett., 148(1), 243–258, https://doi.org/10.1016/S0012-821X(97)00040-X, 1997.

Breiter, K., Lamarão, C. N., Borges, R. M. K., and Dall'Agnol, R.: Chemical characteristics of zircon from A-type granites and comparison to zircon of S-type granites, Lithos, 192–195, 208–225, https://doi.org/10.1016/j.lithos.2014.02.004, 2014.

Castillo, P. R., Janney, P. E., and Solidum, R. U.: Petrology and geochemistry of Camiguin Island, southern Philippines: Insights to the source of adakites and other

727 lavas in a complex arc setting, Contrib. Mineral. Petrol., 134(1), 33–51,
728 https://doi.org/10.1007/s004100050467, 1999.
729 Castro, A., Moreno-Ventas, I., and Rosa, J.: H-type (hybrid) granitoids: a proposed
730 revision of the granite-type classification and nomenclature, Earth. Sci. Rev., 31,
731 237–253, https://doi.org/10.1016/0012-8252(91)90020-G, 1991.
732 Chappell, B. W., and White, A. J. R.: I-and S-type granites in the Lachlan Fold Belt,
733 Geol. Soc. Am. Spec. Pap., 272, 1–26, https://doi.org/10.1130/SPE272-p1, 1992.
734 Chen, S. R., Wang, Q., Zhu, D. C., Weinberg, R. F., Zhang, L. L., and Zhao, Z. D.:
735 Reheating and magma mixing recorded by zircon and quartz from high-silica
736 rhyolite in the Coqen region, southern Tibet, Am. Miner.,
737 https://doi.org/10.2138/am-2020-7426, 2020.
738 Chu, Y., Lin, W., Faure, M., Allen, M. B., and Feng, Z.: Cretaceous exhumation of the
739 Triassic intracontinental Xuefengshan Belt: Delayed unroofing of an orogenic
740 plateau across the South China Block? Tectonophysics, 793, 228592,
741 https://doi.org/1016/j.tecto.2020.228592, 2020.
742 Claiborne, L. L., Miller, C. F., Walker, B. A., Wooden, J. L., Mazdab, F. K., and Bea,
743 F.: Tracking magmatic processes through Zr/Hf ratios in rocks and Hf and Ti
744 zoning in zircons: An example from the Spirit Mountain batholith, Nevada.
745 Mineral. Mag., 70, 517–543, https://doi.org/10.1180/0026461067050348, 2006.
746 Collins, W. J., Beams, S. D., White, A. J. R., and Chappell, B. W.: Nature and origin
747 of A-type granites with particular reference to southeastern Australia, Contrib.
748 Mineral. Petr., 80, 189-200, https://doi.org/10.1007/BF00374895, 1982.

749 Collins, W. J., Huang, H. Q., and Jiang, X. Y.: Water-fluxed crustal melting produces
750 Cordilleran batholiths, Geology, 44(2), 143–146,
751 https://doi.org/10.1130/G37398.1, 2016.
752 Conrad, W. K., Nicholls, I. A., and Wall, V. J.: Water-saturated and -undersaturated
753 melting of metaluminous and peraluminous crustal compositions at 10 kb:
754 evidence for the origin of silisic magmas in the Taupo Volcanic Zone, New
755 Zealand, and other occurrences, J. Petrol., 29, 765–803,
756 https://doi.org/10.1093/petrology/29.4.765, 1988.
757 Defant, M. J., and Drummond, M. S.: Derivation of some modern arc magmas by
758 melting of young subducted lithosphere, Nature, 347, 662–665,
759 https://doi.org/10.1038/347662a0, 1990.
760 Douce, A. E. P.: Generation of metaluminous A-type granites by low-pressure melting
761 of calc-alkaline granitoids, Geology, 25, 743–746, https://doi.org/10.1130/0091-
762 7613(1997)025<0743:GOMATG>2.3.CO;2, 1997.
763 Drummond, M. S., Defant, M. J., and Kepezhinskas, P. K.: Petrogenesis of slab-derived
764 trondhjemite–tonalite–dacite/adakite magmas, Trans. R. Soc. Edinb., 87, 205–215,
765 https://doi.org/10.1017/S0263593300006611, 1996.
766 Faure, M., Lin, W., Moni, P., and Bruguier, O.: Paleoproterozoic arc magmatism and
767 collision in Liaodong Peninsula, NE China, Terra. Nova., 16, 75–80,
768 https://doi.org/10.1111/j.1365-3121.2004.00533.x, 2004.
769 Ferry, J. M., and Watson, E. B.: New thermodynamic models and revised calibrations
770 for the Ti-in-zircon and Zr-in-rutile thermometers, Contrib. Mineral. Petrol., 154,

429–437, https://doi.org/10.1007/s00410-007-0201-0, 2007.

Frost, B. R., Barnes, C. G., Collins, W. J., Arculus, R. J., Ellis, D. J., and Frost, C. D.: A geochemical classification for granitic rocks, J. Petrol., 42, 2033–2048, https://doi.org/10.1093/petrology/42.11.2033, 2001.

Gao, S., Rudnick, R. L., Yuan, H. L., Liu, X. M., Liu, Y. S., Xu, W. L., Ling, W. L., Ayers, J. C., Wang, X. C., and Wang, Q. H.: Recycling lower continental crust in the North China craton, Nature, 432, 892–897, https://doi.org/10.1038/nature03162, 2004.

Gao, Y. F., Hou, Z. Q., Kamber, B. S., Wei, R. H., Meng, X.J., and Zhao, R. S.: Adakite-like porphyries from the southern Tibetan continental collision zones: evidence for slab melt metasomatism, Contrib. Mineral. Petr., 153, 105–20, 10.1007/s00410-006-0137-9, 2007.

Griffin, W. L., Belousova, E. A., Shee, S. R., Pearson, N. J., and O'Reilly, S. Y.: Archean crustal evolution in the northern Yilgarn Craton: U-Pb and Hf-isotope evidence from detrital zircons, Precambrian. Res., 131, 231–282, https://doi.org/10.1016/J.PRECAMRES.2003.12.011, 2004.

He, P. L., Huang, X. L., Yang, F., and Wang, X.: Mineralogy constraints on magmatic processes controlling adakitic features of Early Permian high-magnesium diorites in the Western Tianshan orogenic belt, J. Petrol., 61, a114, https://doi.org/10.1093/petrology/egaa114, 2021.

Hoskin, P. W. O.: Trace-element composition of hydrothermal zircon and the alteration of Hadean zircon from the Jack Hills, Australia, Geochim. Cosmochim. Ac., 69,

637–648, https://doi.org/10.1016/j.gca.2004.07.006, 2005.

Hoskin, P. W., and Schaltegger, U.: The composition of zircon and igneous and metamorphic petrogenesis, Rev. Mineral. Geochem., 53, 27–62, https://doi.org/10.2113/0530027, 2003.

Huang, F., and He, Y.S.: Partial melting of the dry mafic continental crust: Implications for petrogenesis of C-type adakites, Chinese. Sci. Bull., 55, 1255–1267, https://doi.org/10.1007/s11434-010-3224-2, 2010.

Jackson, S. E., Pearson, N. J., Griffin W L, and Belousova, E. A.: The application of laser ablation-inductively coupled plasma-mass spectrometry to in situ U-Pb zircon geochronology, Chem. Geol., 211(1-2), 47–69, https://doi.org/doi:10.1016/j.chemgeo.2004.06.017, 2004.

Jiang, H., Jiang, S. Y., Li, W. Q., Zhao, K. D., and Peng, N. J.: Highly fractionated Jurassic I-type granites and related tungsten mineralization in the Shirenzhang deposit, northern Guangdong, South China: Evidence from cassiterite and zircon U-Pb ages, geochemistry and Sr-Nd-Pb-Hf isotopes, Lithos, S480187509, https://doi.org/10.1016/j.lithos.2018.04.030, 2018.

Jiang, Y.H., Jiang, S.Y., Zhao, K.D., Ni, P., Ling, H.F., and Liu, D.Y.: SHRIMP U-Pb zircon dating for lamprophyre from Liaodong Peninsula: Constraints on the initial time of Mesozoic lithosphere thinning beneath eastern China, Chinese. Sci. Bull., 50, https://doi.org/10.1360/982005-373, 2612–2620, 2005.

Kamei, A., Miyake, Y., Owada, M., and Kimura, J.: A pseudo adakite derived from partial melting of tonalitic to granodioritic crust, Kyushu, southwest Japan arc,

Lithos, 112, 615–625, https://doi.org/10.1016/j.lithos.2009.05.024, 2009.

Kay, R. W., and Kay, S. M.: Delamination and delamination magmatism, Tectonophysics, 219, 177–189, https://doi.org/10.1016/0040-1951(93)90295-U, 1993.

King, S. D., Frost, D. J., and Rubie D. C.: Why cold slabs stagnate in the transition zone, Geology, 43(3), 231–234, https://doi.org/10.1130/G36320.1, 2015.

Li, C.M., Zhang, C.H., Cope, T.D., and Lin, Y.: Out-of-sequence thrusting in polycyclic thrust belts: An example from the Mesozoic Yanshan belt, North China Craton, Tectonics, 35, 2082–2116, https://doi.org/10.1002/2016TC004187, 2016.

Li, S. Z., and Zhao, G. C.: SHRIMP U-Pb zircon geochronology of the Liaoji granitoids: Constraints on the evolution of the Paleoproterozoic Jiao-Liao-Ji belt in the Eastern Block of the North China Craton, Precambrian. Res., 158, 1–16, https://doi.org/10.1016/j.precamres.2007.04.001, 2007.

Li, S. Z., Zhao, G. C., Sun, M., Han, Z. Z., Hao, D. F., Luo, Y., and Xia, X. P.: Deformation history of the Paleoproterozoic Liaohe Group in the Eastern Block of the North China Craton, J. Asian. Earth. Sci., 24, 659–674, https://doi.org/659–67410.1016/j.jseaes.2003.11.008, 2005.

Li, S.Z., Liu, J.Z., Zhao, G.C., Wu, F.Y., Han, Z.Z., and Yang, Z.Z.: Key geochronology of Mesozoic deformation in the eastern block of the North China Craton and its constraints on regional tectonics: A case of Jiaodong and Liaodong Peninsula, Acta. Petrol. Sin., 2, 633–646, https://doi.org/10.1007/BF02873097, 2004.

837 Li, X.H., Long, W.G., Li, Q.L., Liu, Y., Zheng, Y.F., Yang, Y.H., Chamberlain, K.R.,
838 Wan, D.F., Guo, C.H., and Wang, X.C.: Penglai Zircon Megacrysts: A Potential
839 New Working Reference Material for Microbeam Determination of Hf-O Isotopes
840 and U-Pb Age, Geostand. Geoanal. Res., 34, 117–134,
841 https://doi.org/info:doi/10.1111/j.1751-908X.2010.00036.x, 2010.
842 Li, Z., Chen, B., Liu, J.W., Zhang, L., and Yang, C.: Zircon U-Pb ages and their
843 implications for the South Liaohe Group in the Liaodong Peninsula, Northeast
844 China (in Chinese with English abstract), Acta. Petrol. Sin., 31(6), 1589–1605,
845 2015.
846 Liu, Y.S., Hu, Z.C., Zong, K.Q., Gao, C.G., Gao, S., Xu, J., and Chen, H.H.:
847 Reappraisement and refinement of zircon U-Pb isotope and trace element analyses
848 by LA-ICP-MS, Chinese. Sci. Bull., 55, 1535–1546,
849 https://doi.org/10.1007/s11434-010-3052-4, 2010.
850 Loader, M. A., Wilkinson, J. J., and Armstrong, R. N.: The effect of titanite
851 crystallisation on Eu and Ce anomalies in zircon and its implications for the
852 assessment of porphyry Cu deposit fertility, Earth. Planet. Sc. Lett., 472, 107–119,
853 https://doi.org/10.1016/j.epsl.2017.05.010, 2017.
854 Ludwig, K. R.: User's manual for Isoplot 3.00: a geochronological toolkit for Microsoft
855 Excel, Berkeley. Geochronology. Center., 2003.
856 Ma, L., Jiang, S.Y., Dai, B.Z., Jiang, Y.H., Hou, M.L., Pu, W., and Xu, B.: Multiple
857 sources for the origin of Late Jurassic Linglong adakitic granite in the Shandong
858 Peninsula, eastern China: Zircon U-Pb geochronological, geochemical and Sr-Nd-

Hf isotopic evidence, Lithos, 162–163, 251–263, https://doi.org/10.1016/j.lithos.2013.01.009, 2013b.

Ma, Q., Zheng, J.P., Griffin, W. L., Zhang, M., Tang, H.Y., Su, Y.P., and Ping, X.Q.: Triassic “adakitic” rocks in an extensional setting (North China): Melts from the cratonic lower crust, Lithos, 149, 159–173, https://doi.org/ 10.1016/j.lithos.2012.04.017, 2012.

Ma, Q., Zheng, J.P., Xu, Y.G., Griffin, W. L., and Zhang, R.S.: Are continental “adakites” derived from thickened or foundered lower crust? Earth. Planet. Sc. Lett., 419, 125–133, https://doi.org/10.1016/j.epsl.2015.02.036, 2015.

Ma, X.H., Chen, B., and Yang, M.C.: Magma mixing origin for the Aolunhua porphyry related to Mo-Cu mineralization, eastern Central Asian Orogenic Belt, Gondwana. Res., 24, 1152–1171, https://doi.org/10.1016/j.gr.2013.02.010, 2013a.

Macpherson, C. G., Dreher, S. T., and Thirlwall, M. F.: Adakites without slab melting: High pressure differentiation of island arc magma, Mindanao, the Philippines, Earth. Planet. Sc. Lett., 243(3), 581–593, https://doi.org/10.1016/j.epsl.2005.12.034, 2006.

Mahon, K. I.: The New “York” regression: Application of an improved statistical method to geochemistry, Int. Geol. Rev., 38(4), 293–303, https://doi.org/10.1080/00206819709465336, 1996.

Maniar, P. D., and Piccoli, P. M.: Tectonic discrimination of granitoids, Geol. Soc. Am. Bull., 101, 635–643, https://doi.org/10.1130/0016-7606(1989)101<0635:TDOG>2.3.CO;2, 1989.

881 Martin, H., Smithies, R.H., Rapp, R., Moyen, J.-F., and Champion, D.: An overview of
882 adakite, tonalite-trondhjemite-granodiorite (TTG), and sanukitoid: relationships
883 and some implications for crustal evolution, Lithos, 79, 1–24,
884 https://doi.org/10.1016/j.lithos.2004.04.048, 2005.
885 Meng, E., Liu, F.L., Liu, P.H., Liu, C.H., Yang, H., Wang, F., Shi, J.R., and Cai, J.:
886 Petrogenesis and tectonic significance of Paleoproterozoic meta-mafic rocks from
887 central Liaodong Peninsula, northeast China: Evidence from zircon U-Pb dating
888 and in situ Lu-Hf isotopes, and whole-rock geochemistry, Precambrian. Res., 247,
889 92–109, https://doi.org/10.1016/j.precamres.2014.03.017, 2014.
890 Meng, Q. R.: What drove late Mesozoic extension of the northern China-Mongolia tract?
891 Tectonophysics, 369, 155–174, https://doi.org/0.1016/S0040-1951(03)00195-1,
892 2003.
893 Mezger, K., and Krogstad, E. J.: Interpretation of discordant U-Pb zircon ages: An
894 evaluation, J. Metamorph. Geol., 15, 127–140, https://doi.org/10.1111/j.1525-
895 1314.1997.00008.x,1997.
896 Miller, C. F., McDowell, S. M., and Mapes, R. W.: Hot and cold granites? Implications
897 of zircon saturation temperatures and preservation of inheritance, Geology, 31,
898 529–532, https://doi.org/10.1130/0091-7613(2003)031<0529:hacgio>2.0.co;2,
899 2003.
900 Miller, J.F., and Harris, N.B.W.: Evolution of continental crust in the Central Andes;
901 constraints from Nd isotope systematics, Geology, 17, 615–617,
902 https://doi.org/10.1130/0091-7613(1989)0172.3.CO;2, 1989.

903 Moyen, J.: High Sr/Y and La/Yb ratios: The meaning of the “adakitic signature”, Lithos,
904 112, 556–574, https://doi.org/10.1016/j.lithos.2009.04.001, 2009.
905 Nakamura, H., and Iwamori, H.: Generation of adakites in a cold subduction zone due
906 to double subducting plates, Contrib. Mineral. Petr., 165, 1107–1134,
907 https://doi.org/10.1007/s00410-013-0850-0, 2013.
908 Nasdala, L., Pidgeon, R. T., Wolf, D., and Irmer, G., Metamictization and U-Pb isotopic
909 discordance in single zircons: a combined Raman microprobe and SHRIMP ion
910 probe study, Miner. Petrol., 62, 1–27, https://doi.org/10.1007/BF01173760, 1998.
911 Nash, D.J., Ciborowski, T., Ullyott, J.S., Pearson, M.P. and Whitaker, K.A.: Origins of
912 the sarsen megaliths at Stonehenge, Sci. Adv., 6, eabc0133,
913 https://doi.org/10.1126/sciadv.abc0133, 2020.
914 Ou, Q., Wang, Q., Wyman, D. A., Zhang, H.X., Yang, J.H., Zeng, J.P., Hao, L.L., Chen,
915 Y.W., Liang, and H., Qi, Y.: Eocene adakitic porphyries in the central-northern
916 Qiangtang Block, central Tibet: Partial melting of thickened lower crust and
917 implications for initial surface uplifting of the plateau, J. Geophys. Res. Solid.
918 Earth., 122, 1025–1053, https://doi.org/10.1002/2016JB013259, 2017.
919 Parsons, B., and Dan, M.K.: Mantle convection and the thermal structure of the plates,
920 J. Geophys. Res. Solid. Earth., 83, https://doi.org/10.1029/JB083iB09p04485,
921 1978.
922 Patiño Douce, A.E.P.: What do experiments tell us about the relative contributions of
923 crust and mantle to the origin of granitic magmas? Geol. Soc. Lond. Spec. Publ.,
924 168(1), 55–75, https://doi.org/10.1144/GSL.SP.1999.168.01.05, 1999.

925 Qiu, L., Kong, R.Y., Yan, D.P., Wells, M.L., Wang, A.P., Sun, W.H., Yang, W.X., Han,
926 Y.G., Li, C.M., and Zhang, Y.X.: The Zhayao tectonic window of the Jurassic
927 Yuantai thrust system in Liaodong Peninsula, NE China: Geometry, kinematics
928 and tectonic implications, J. Asian Earth Sci., 164, 58–71, https://doi.org/
929 10.1016/j.jseaes.2018.06.012, 2018.
930 Rapp, R. P., Shimizu, N and Norman, M.D.: Growth of early continental crust by partial
931 melting of eclogite, Nature, 425(6958), 605–609,
932 https://doi.org/10.1038/nature02031, 2003.
933 Ren, Z.H., Lin, W., Faure, M., Meng, L.T., Qiu, H.B., and Zeng, J.P.: Triassic- Jurassic
934 evolution of the eastern North China Craton: Insights from the Lushun-Dalian area,
935 South Liaodong Peninsula, NE China, Geol. Soc. Am. Bull., 133(1–2),
936 https://doi.org/10.1130/B35533.1, 2020.
937 Rudnick, R. L., and Gao, S.: Composition of the continental crust, Treatise. Geochem.,
938 3, 1–64, https://doi.org/10.1016/b0-08-043751-6/03016-4, 2003.
939 Schiller, D., and Finger, F.: Application of Ti-in-zircon thermometry to granite studies:
940 problems and possible solutions, Contrib. Mineral. Petr., 174,
941 https://doi.org/10.1007/s00410-019-1585-3, 2019.
942 Schmitz, M. D., and Kuiper, K. F.: High-Precision Geochronology, Elements., 9, 25–
943 30, https://doi.org/10.2113/gselements.9.1.25, 2013.
944 Schwartz, J. J., Johnson, K., Miranda, E. A., and Wooden, J. L.: The generation of high
945 Sr/Y plutons following Late Jurassic arc–arc collision, Blue Mountains province,
946 NE Oregon, Lithos, 126, 22–41, https://doi.org/10.1016/j.lithos.2011.05.005,

947 2011.
948 Scott, E.M., Allen, M.B., Macpherson, C.G., McCaffrey, K.J.W., Davidson, J.P.,
949 Saville, C., and Ducea, M.N.: Andean surface uplift constrained by radiogenic
950 isotopes of arc lavas, Nat. Commun., 9(1), 969, https://doi.org/10.1038/s41467-
951 018-03173-4, 2018.
952 Shahbazi, H., Maghami, Y. T., Azizi, H., Asahara, Y., Siebel, Y., Maanijou, M., and
953 Rezai, A.: Zircon U-Pb ages and petrogenesis of late Miocene adakitic rocks from
954 the Sari Gunay gold deposit, NW Iran, Geol. Mag.,
955 https://doi.org/10.1017/S0016756821000297, 2021.
956 Shannon. R.D.: Revised effective ionic radii and systematic studies of interatomic
957 distances in halides and chalcogenides, Acta. Crystall. A., 32(5), 751–767,
958 https://doi.org/10.1107/S0567739476001551, 1976.
959 Shaw, D.M.: Trace element fractionation during anatexis, Geochim. Cosmochim. Ac.,
960 34, 237–243, https://doi.org/10.1016/0016-7037(70)90009-8, 1970.
961 Siégel, C., Bryan, S. E., Allen, C. M., and Gust, D. A.: Use and abuse of zircon-based
962 thermometers: A critical review and a recommended approach to identify
963 antecrystic zircons, Earth. Sci. Rev., 176, 87–116,
964 https://doi.org/10.1016/j.earscirev.2017.08.011, 2018.
965 Skjerlie, K. P., and Johnston, A. D.: Vapor-absent melting at 10 kbar of a biotite-and
966 amphibole-bearing tonalitic gneiss: implications for the generation of A-type
967 granites, Geology, 20, 263–266, https://doi.org/10.1130/0091-
968 7613(1992)0202.3.CO;2, 1992.

969 Sláma, J., Košler, J., and Condon, D. J.: Plešovice zircon-A new natural reference
970 material for U-Pb and Hf isotopic microanalysis, Chem. Geol., 249(1–2), 1–35,
971 https://doi.org/doi:10.1016/j.chemgeo.2007.11.005, 2008.
972 Söderlund, U., Patchett, P.J., Vervoort, J.D., and Isachsen, C.E.: The 176 Lu decay
973 constant determined by Lu-Hf and U-Pb isotope systematics of Precambrian mafic
974 intrusions, Earth. Planet. Sc. Lett., 219(3), 311–324,
975 https://doi.org/10.1016/S0012-821X(04)00012-3, 2004.
976 Sun, S. S., and McDonough, W. F.: Chemical and isotopic systematics of oceanic
977 basalts: implications for mantle composition and processes, Geol. Soc. Lond. Spec.
978 Publ., 42, 313–345, https://doi.org/10.1144/GSL.SP.1989.042.01.19, 1989.
979 Tang. J., Xu. W. L., Wang. F., and Ge. W.C.: Subduction history of the Paleo-Pacific
980 slab beneath Eurasian continent: Mesozoic-Paleogene magmatic records in
981 Northeast Asia, Sci. China. Earth. Sci., 61, 527–559,
982 https://doi.org/CNKI:SUN:JDXG.0.2018-05-003, 2018.
983 Trail, D., Watson, E. B., and Tailby, N. D.: Ce and Eu anomalies in zircon as proxies
984 for the oxidation state of magmas, Geochim. Cosmochim. Ac., 97, 70–87,
985 https://doi.org/10.1016/j.gca.2012.08.032, 2012.
986 Vervoort, J.D., and Blichert-Toft, J.: Evolution of the depleted mantle: Hf isotope
987 evidence from juvenile rocks through time, Geochim. Cosmochim. Ac., 63(3),
988 533–556, https://doi.org/10.1016/S0016-7037(98)00274-9, 1999.
989 Wan, Y.S., Song, B., Liu, D.Y., Wilde, S. A., Wu, J.S., Shi, Y.R., Yin, X.Y., and Zhou,
990 H.Y.: 2006. SHRIMP U-Pb zircon geochronology of Palaeoproterozoic

991 metasedimentary rocks in the North China Craton: Evidence for a major Late
992 Palaeoproterozoic tectonothermal event, Precambrian. Res., 149, 271,
993 https://doi.org/10.1016/j.precamres.2006.06.006, 2006.
994 Wang, F., Liu, F., Schertl, H.P., Xu, W., Liu, P., and Tian, Z.: Detrital zircon U-Pb
995 geochronology and Hf isotopes of the Liaohe Group, Jiao-Liao-Ji Belt:
996 Implications for the Paleoproterozoic tectonic evolution, Precambrian. Res., 340,
997 105633, 10.1016/j.precamres.2020.105633, 2020b.
998 Wang, N., Wu, C. L, Lei, M., and Chen, H.J.: Petrogenesis and tectonic implications of
999 the Early Paleozoic granites in the western segment of the North Qilian orogenic
1000 belt, China, Lithos, 312–313, 89–107, https://doi.org/10.1016/j.lithos.2018.04.023,
1001 2018.
1002 Wang, Q., Xu, J. F., Jian, P., Bao Z. W., Zhao. Z. H., Li. C. F., Xiong. X. L., and Ma,
1003 J. L.: Petrogenesis of adakitic porphyries in an extensional tectonic setting, Dexing,
1004 South China: Implications for the genesis of porphyry copper mineralization, J.
1005 Petrol., 47(1), 119–144, https://doi.org/10.1093/petrology/egi070, 2006.
1006 Wang, X. P., Oh, C. W., Peng, P., Zhai, M. G., Wang, X. H., and Lee, B. Y.:
1007 Distribution pattern of age and geochemistry of 2.18-2.14 Ga I- and A-type
1008 granites and their implication for the tectonics of the Liao-Ji belt in the North
1009 China Craton, Lithos, 364–365, 105518,
1010 https://doi.org/10.1016/j.lithos.2020.105518, 2020a.
1011 Wang, X., Griffin, W. L., Chen, J., Huang, P.Y., and Li, X.: U and Th contents and
1012 Th/U ratios of zircon in felsic and mafic magmatic rocks: Improved zircon-melt

1013 distribution coefficients, Acta. Geol. Sin. Engl., 85, 164–174,
1014 https://doi.org/10.1111/j.1755-6724.2011.00387.x, 2011.
1015 Wang, X., Griffin, W. L., O'Reilly, S. Y., and Li, W.X.: Three stages of zircon growth
1016 in magmatic rocks from the Pingtan Complex, eastern China, Acta. Geol. Sin.
1017 Engl., 81, 68–80, https://doi.org/10.3321/j.issn:1000-9515.2007.01.008, 2007.
1018 Wang, X.L., Lv, X., Liu, Y.J., Zhao, Y.Y., Li, C., Wu, W.B., Wang, Y.P., and Li, H.Y.:
1019 LA-ICP-MS zircon U-Pb ages, geochemical characteristics of Late Triassic
1020 intrusives in Xiuyan area, eastern Liaoning and their geological significances, Ore.
1021 Geol. Rev., 65, 401–416, https://doi.org/10.16509/j.georeview.2019.02.010, 2019.
1022 Watson, E. B., and Harrison, T. M.: Zircon saturation revisited: temperature and
1023 composition effects in a variety of crustal magma types, Earth. Planet. Sci. Lett.,
1024 64, 295–304, https://doi.org/10.1016/0012-821X(83)90211-X, 1983.
1025 Watson, E. B., and Harrison, T. M.: Zircon thermometer reveals minimum melting
1026 conditions on earliest Earth, Science, 308, 841–844,
1027 https://doi.org/10.1126/science.1110873, 2005.
1028 Whalen, J. B., Currie, K. L., and Chappell, B. W.: A-type granites: geochemical
1029 characteristics, discrimination and petrogenesis, Contrib. Mineral. Petr., 95, 407–
1030 419, https://doi.org/10.1007/BF00402202, 1987.
1031 Wolf, M. B., and London, D.: Apatite dissolution into peraluminous haplogranitic melts:
1032 An experimental study of solubilities and mechanisms, Geochim. Cosmochim.
1033 Acta., 58, 4127–4145. https://doi.org/10.1016/0016-7037(94)90269-0, 1994.
1034 Wu, F. Y., Jahn, B. M., Wilde, S. A., Lo, C. H., Yui, T. F., Lin, Q., Ge, W. C., and Sun,

1035 D. Y: Highly fractionated I-type granites in NE China (I): geochronology and
1036 petrogenesis, Lithos, 66, 241–273, https://doi.org/10.1016/s0024-4937(02)00222-
1037 0, 2003.
1038 Wu, F. Y., Liu, X. C., Ji, W. Q., Wang, J. M., and Yang, L.: Highly fractionated granites:
1039 Recognition and research, Sci. China. Earth. Sci., 60, 1201–1219,
1040 https://doi.org/10.1007/s11430-016-5139-1, 2017.
1041 Wu, F. Y., Yang, J. H., and Liu, X. M.: Geochronological framework of the Mesozoic
1042 granitic magmatism in the Liaodong Peninsula, Northeast China (in Chinese with
1043 English abstract), Geol. J. China. Univ., 11, 305–317, 2005b.
1044 Wu, F.Y., Han, R.H., Yang, J.H., Wilde, S. A., Zhai, M.G., and Park, S. C.: Initial
1045 constraints on the timing of granitic magmatism in North Korea using U-Pb zircon
1046 geochronology, Chem. Geol., 238, 232–248,
1047 https://doi.org/10.1016/j.chemgeo.2006.11.012, 2007.
1048 Wu, F.Y., Lin, J.Q., Wilde, S. A., Zhang, X.O., and Yang, J.H.: Nature and significance
1049 of the Early Cretaceous giant igneous event in eastern China, Earth. Planet. Sci.
1050 Lett., 233, 103–119, https://doi.org/10.1016/j.epsl.2005.02.019, 2005c.
1051 Wu, F.Y., Yang, J.H., Wilde, S. A., and Zhang, X.O.: Geochronology, petrogenesis and
1052 tectonic implications of Jurassic granites in the Liaodong Peninsula, NE China,
1053 Chem. Geol., 221, 127–156, https://doi.org/10.1016/j.chemgeo.2005.04.010,
1054 2005a.
1055 Wu, F.Y., Yang, Y.H., Xie, L.W., Yang, J.H., and Xu, P.: Hf isotopic compositions of
1056 the standard zircons and baddeleyites used in U-Pb geochronology, Chem. Geol.,

234, 105–126, https://doi.org/10.1016/j.chemgeo.2006.05.003, 2006.

Xu, J. F., Shinjo, R., Defant, M. J., Wang, Q., and Rapp, R. P.: Origin of Mesozoic adakitic intrusive rocks in the Ningzhen area of east China: partial melting of delaminated lower continental crust? Geology, 30(12), 1111–1114, https://doi.org/10.1130/0091-7613(2002)0302.0.CO;2, 2002.

Xue, J. X., Liu, Z. H., Liu, J. X., Dong, X. J., Feng, F., and Lian, G. H.: Geochemistry, Geochronology, Hf isotope and Tectonic Significance of the Late Jurassic Huangdi Pluton in Xiuyan, Liaodong Penins (in Chinese with English abstract), Earth Science, 46(6), 2030–2043, https://doi.org/10.3799/dqkx.2020.008， 2020.

Xue, S., Ling, M. X., Liu, Y. L., Zhang, H., and Sun, W.D.: The genesis of early Carboniferous adakitic rocks at the southern margin of the Alxa Block, North China, Lithos, 278–281, 181–194, https://doi.org/10.1016/j.lithos.2017.01.012, 2017.

Yang, F.C., Song, Y.H., Hao, L.B., and Peng, C.: Late Jurassic SHRIMP U-Pb age and Hf isotopic characteristics of granite from the Sanjiazi Area in Liaodong and their geological significance (in Chinese with English abstract), Acta. Geol. Sin. Engl., 89, 1773–1782, 2015a.

Yang, F.C., Song, Y.H., Yang, J.L., Shen, X., and Gu, Y.C.: SHRIMP U-Pb age and geochemical characteristics of granites in Wulong-Sidaogou Gold Deposit, East Liaoning (in Chinese with English abstract), Geotectonica et Metallogenia, 42, 940–954, https://doi.org/10.16539/j.ddgzyckx.2018.05.010, 2018.

Yang, J. H., Wu, F. Y., Xie, L. W., and Liu, X. M.: Petrogenesis and tectonic

implications of Kuangdonggou synites in the Liaodong Peninsula, east North China Craton: Constraints from in-suit zircon U-Pb ages and Hf isotopes (in Chinese with English abstract), Acta. Petrol. Sin., 23, 263–276, https://doi.org/10.1016/j.sedgeo.2006.03.028, 2007.

Yang, J.H., Wu, F.Y., Lo, C.H., Chung, S.L., Zhang, Y,B., and Wilde, S.A.: Deformation age of Jurassic granites in the Dandong area, eastern China: Ar-40/Ar-39 geochronological constraints (in Chinese with English abstract), Acta. Petrol. Sin., 20(5), 1205–1214, 2004.

Yang, M. C., Chen, B., and Yan, C.: Petrological, geochronological, geochemical and Sr-Nd-Hf isotopic constraints on the petrogenesis of the Shuangcha Paleoproterozoic megaporphyritic granite in the southern Jilin Province: Tectonic implications (in Chinese with English abstract), Acta. Petrol. Sin., 31, 1573–1588, 2015b.

Yang, M.C., Chen, B., and Yan, C.: Paleoproterozoic Gneissic Granites in the Liaoji Mobile Belt, North China Craton: Implications for Tectonic Setting. In: Zhai M., Zhao Y., Zhao T. (eds) Main Tectonic Events and Metallogeny of the North China Craton, Springer. Geology. Springer. Singapore., 155–180, https://doi.org/10.1007/978-981-10-1064-4_7, 2016.

Yu, S., Zhang, J., and Del Real, P. G.: Geochemistry and zircon U-Pb ages of adakitic rocks from the Dulan area of the North Qaidam UHP terrane, north Tibet: constraints on the timing and nature of regional tectonothermal events associated with collisional orogeny, Gondwana. Res., 21, 167–179,

https://doi.org/10.1016/j.gr.2011.07.024, 2012.

Yuan, H.L., Gao, S., Dai, M.N., Zong, C.L., Günther, D., Fontaine, G.H., Liu, X.M., and Diwu, C.R.: Simultaneous determinations of U-Pb age, Hf isotopes and trace element compositions of zircon by excimer laser-ablation quadrupole and multiple-collector ICP-MS, Chem. Geol., 247, 100–118, https://doi.org/10.1016/j.chemgeo.2007.10.003, 2008.

Yuan, L. L., Zhang, X. H., Xue, F. H., Han, C. M., Chen, H. H., and Zhai, M. G.: Two episodes of Paleoproterozoic mafic intrusions from Liaoning province, North China Craton: Petrogenesis and tectonic implications, Precambrian. Res., 264, 119–139, https://doi.org/10.1016/j.precamres.2015.04.017, 2015.

Zeng, R.Y., Lai, J.Q., Mao, X.C., Li, B., Ju, P.J., and Tao, S.L.: Geochemistry, zircon U-Pb dating and Hf isotopies composition of Paleozoic granitoids in Jinchuan, NW China: Constraints on their petrogenesis, source characteristics and tectonic implication, J. Asian. Earth. Sci., 121, 20–33, https://doi.org/10.1016/j.jseaes.2016.02.009, 2016.

Zeng, R.Y., Lai, J.Q., Mao, X.C., Li, B., Zhang, J.D., Bayless, R., and Yang, L.Z.: Paleoproterozoic Multiple Tectonothermal Events in the Longshoushan Area, Western North China Craton and Their Geological Implication: Evidence from Geochemistry, Zircon U-Pb Geochronology and Hf Isotopes, Minerals. Basel., 8, https://doi.org/10.3390/MIN8090361, 2018.

Zhai, M.G., Meng, Q.R., Liu, J.M., Hou, Q.L., Hu, S.B., Li, Z., Zhang, H.F., Liu, W., Shao, J.A., and Zhu, R.X.: Geological features of Mesozoic tectonic regime

1123 inversion in eastern North China and implication for geodynamics, Earth. Science.
1124 Frontiers., 11, 285–298, https://doi.org/10.3321/j.issn:1005-2321.2004.03.027,
1125 2004.
1126 Zhan, Q. Y., Zhu, D. C., Wang, Q., Weinberg, R. F., Xie, J. C., Li, S. M., Zhang, L.L.,
1127 and Zhao, Z. D.: Source and pressure effects in the genesis of the Late Triassic
1128 high Sr/Y granites from the Songpan-Ganzi Fold Belt, eastern Tibetan Plateau,
1129 Lithos, 368–369, https://doi.org/10.1016/j.lithos.2020.105584, 2020.
1130 Zhang, B., Guo, F., Zhang, X. B., Wu, Y.M., Wang, G.Q., and Zhao, L.: Early
1131 Cretaceous subduction of Paleo-Pacific Ocean in the coastal region of SE China:
1132 Petrological and geochemical constraints from the mafic intrusions, Lithos, 334–
1133 335, 8–24, https://doi.org/10.1016/j.lithos.2019.03.010, 2019.
1134 Zhang, Q., Qian, Q., Wang, E.Q., Wang, Y., Zhao, T.P., Hao, J., and Guo, G.J.: An
1135 East China plateau in mid-late Yanshanian period: implication from adakites,
1136 Chinese (in Chinese with English abstract). Chinese Journal of Geology, 36 (2),
1137 248–255, 2001.
1138 Zhang, Q., Wang, Y., Liu, H., and Wang, Y.: On the space-time distribution and
1139 geodynamic environments of adakites in China annex: controversies over differing
1140 opinions for adakites in China (in Chinese with English abstract), Earth Science
1141 Frontiers, https://doi.org/10.1016/S0955-2219(02)00073-0, 2003.
1142 Zhang, S., Zhu, G., Xiao, S.Y., Su, N., Liu, C., Wu, X.D., Yin, H., Li, Y.J., and Lu,
1143 Y.C.: Temporal variations in the dynamic evolution of an overriding plate:
1144 Evidence from the Wulong area in the eastern North China Craton, China, Geol.

1145 Soc. Am. Bull., 132(9–10), 2023–2042, https://doi.org/10.1130/B35465.1, 2020.
1146 Zhao, K.D., Jiang, S.Y., Ling, H.F., and Palmer, M. R.: Reliability of LA-ICP-MS U-
1147 Pb dating of zircons with high U concentrations: A case study from the U-bearing
1148 Douzhashan Granite in South China, Chem. Geol., 389, 110–121,
1149 https://doi.org/10.1016/j.chemgeo.2014.09.018, 2014.
1150 Zhao, K.D., Jiang, S.Y., Ling, H.F., and Palmer, M. R.: Reliability of LA-ICP-MS U-
1151 Pb dating of zircons with high U concentrations: A case study from the U-bearing
1152 Douzhashan Granite in South China, Chem. Geol., 389, 110–121,
1153 https://doi.org/10.1016/j.chemgeo.2014.09.018, 2014.
1154 Zheng, J.P., and Dai, H.K.: Subduction and retreating of the western Pacific plate
1155 resulted in lithospheric mantle replacement and coupled basinmountain respond in
1156 the North China Craton, Sci. China. Earth. Sci., 61, 406–424,
1157 https://doi.org/10.1007/s11430-017-9166-8, 2018.
1158 Zheng, Y.F., Xu, Z.F., Zhao, Z.F., and Dai, L.Q.: Mesozoic mafic magmatism in North
1159 China: Implications for thinning and destruction of cratonic lithosphere, Sci. China.
1160 Earth Sci., 61, 353–385, https://doi.org/10.1007/s11430-017-9160-3, 2018.
1161 Zhu, R. X., and Xu, Y. G.: The subduction of the west Pacific plate and the destruction
1162 of the North China Craton, Sci. China. Earth Sci., 62, https://doi.org/1340-1350,
1163 10.1007/s11430-018-9356-y, 2019.
1164 Zhu, R.X., and Xu, Y.G.: The subduction of the west Pacific plate and the destruction
1165 of the North China Craton, Sci. China. Earth. Sci., 62, 1340–1350,
1166 https://doi.org/10.1007/s11430-018-9356-y, 2019.

Table captions

Table S1. Major element (wt. %) and trace element (ppm) compositions of the Zhoujiapuzi granite

Table S2. Raman microprobe data

Table S3. The zircon major element (wt. %) and trace element (ppm) from the Zhoujiapuzi granite

Table S4. Zircon La-ICP-MS U-Pb isotopic data and ages of the Zhoujiapuzi granite

Table S5. Zircon Hf isotopic data of the Zhoujiapuzi granite

Figure captions

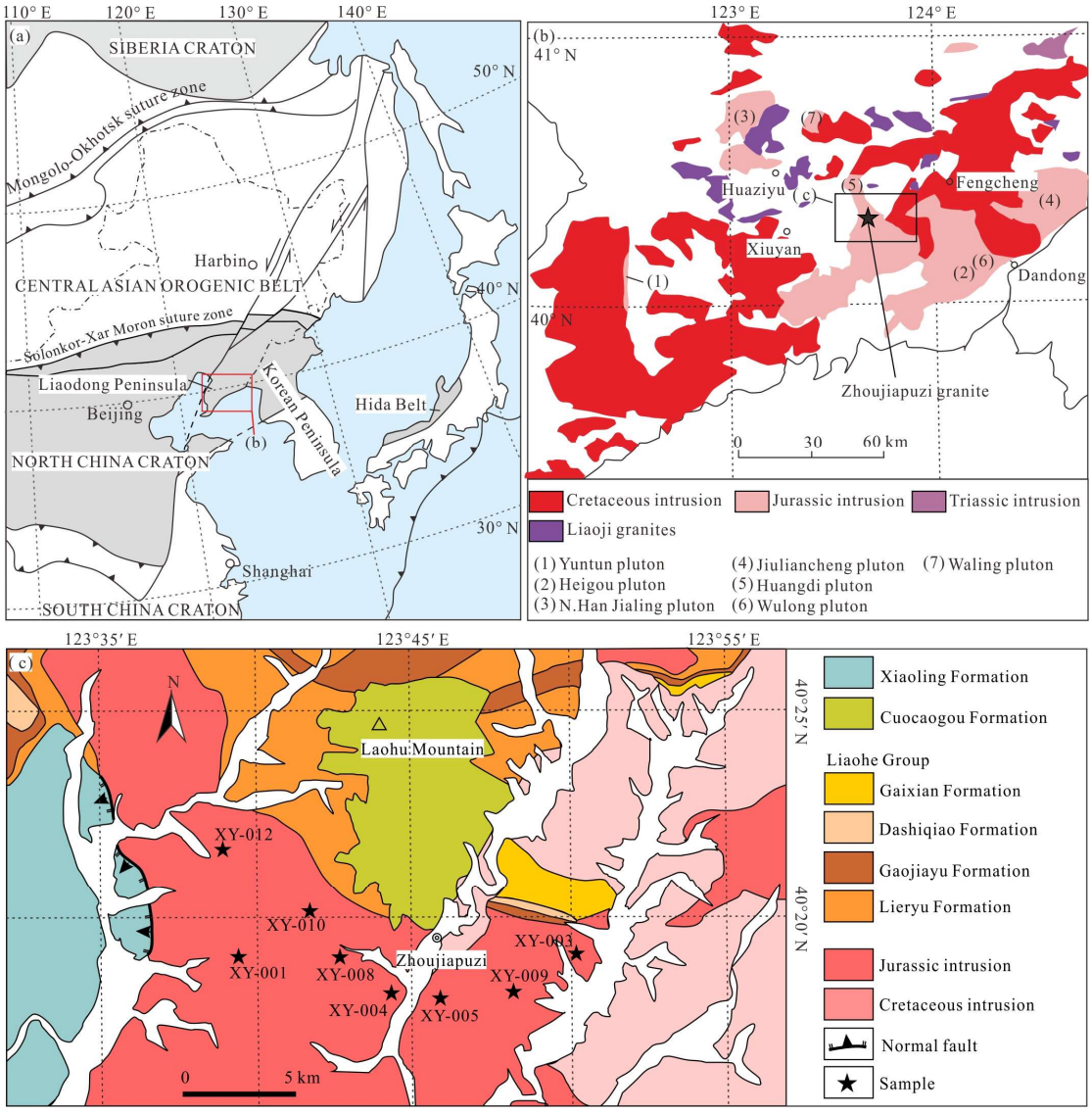

Figure 1. (a) Simplified geological map of Northeast China (Modified from Li et al., 2016); (b) distribution of Mesozoic intrusions in the Liaodong Peninsula (Modified from Wu et al., 2005a); (c) geological map of the Zhoujiapuzi granite.

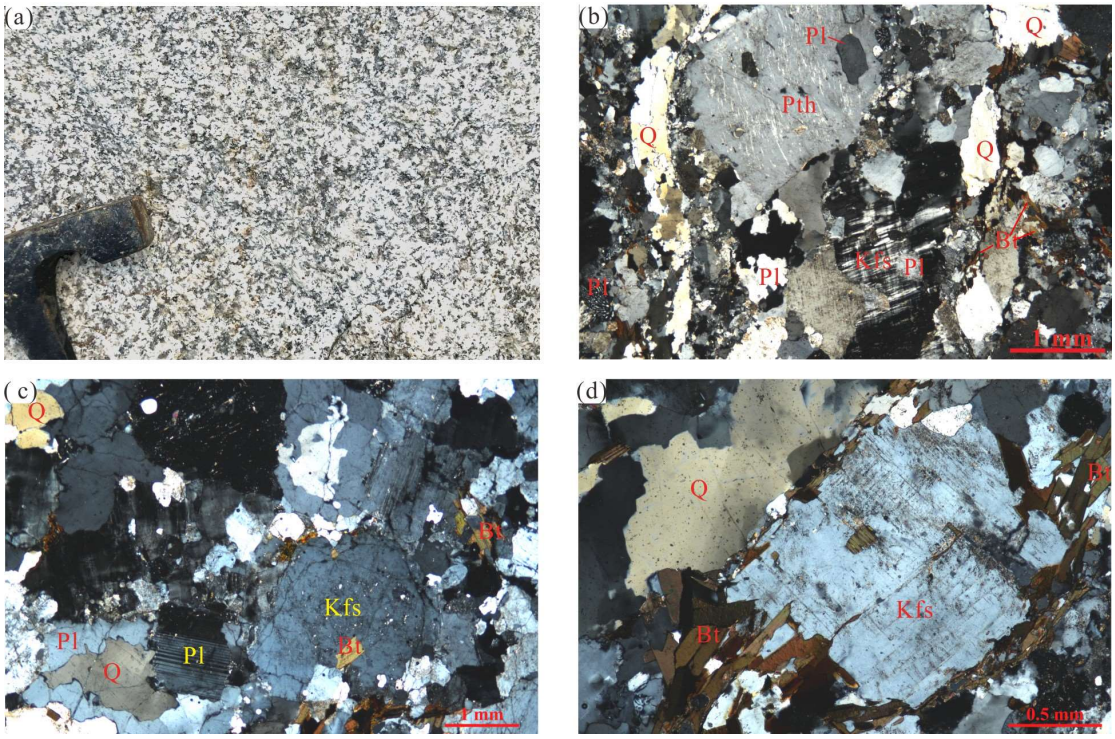

1182

1183 Figure 2. Outcrop photograph (a) and corresponding micrographs (b, c, d-

1184 perpendicular polarized light). Q quartz; Kfs feldspar; Pl plagioclase; Pth perthite; Bt

1185 biotite

1186

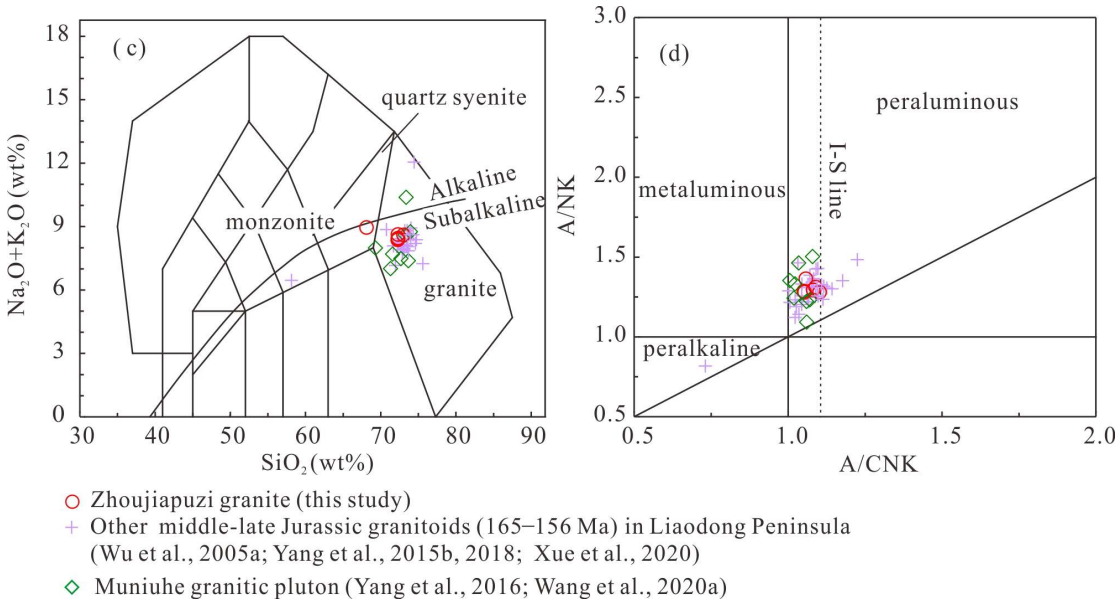

1187

1188 Figure 3. Geochemical classification diagrams for the Zhoujiapuzi granite. (a) TAS

1189 diagram (after Frost et al.， 2001); (b)A/CNK-A/NK diagram (after Maniar and

Piccoli, 1989)

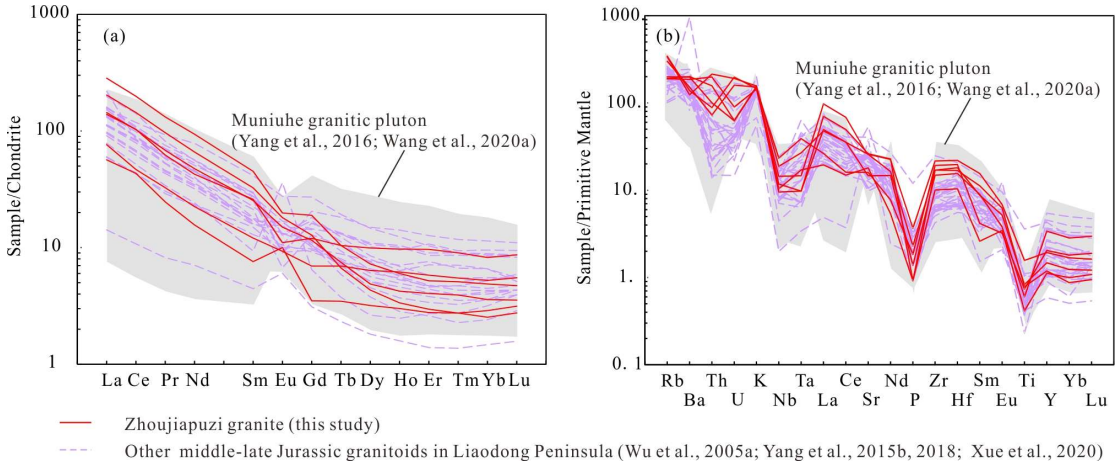

Figure 4. Chondrite-normalized REE patterns and primitive mantle-normalized trace element patterns of the Zhoujiapuzi granite (chondrite and primitive mantle values are from Sun and McDonough, 1989).

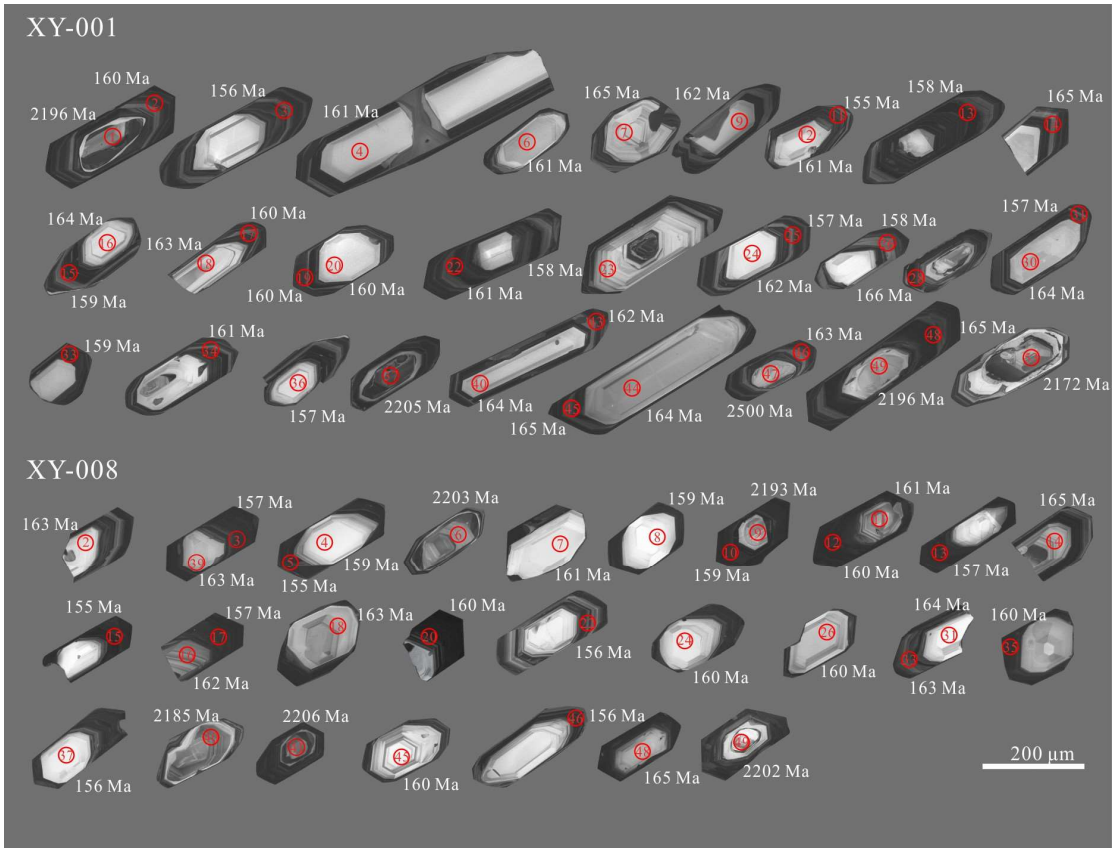

Figure 5. CL images of zircons. Circles denote U-Pb analysis spot. Numbers in the

circles are the spot numbers. Numbers near the analytical spots are the U–Pb ages (Ma).

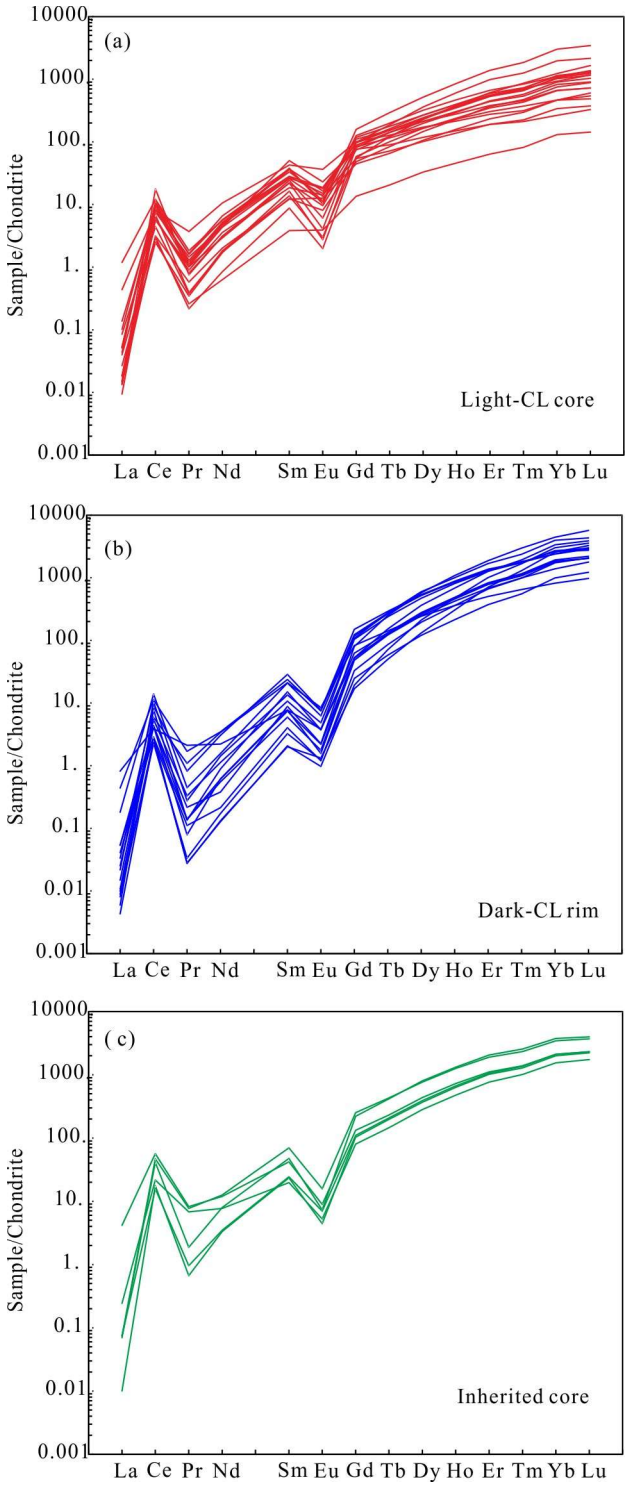

Figure 6. Chondrite-normalized REE patterns of zircon (chondrite values are from Sun and McDonough, 1989).

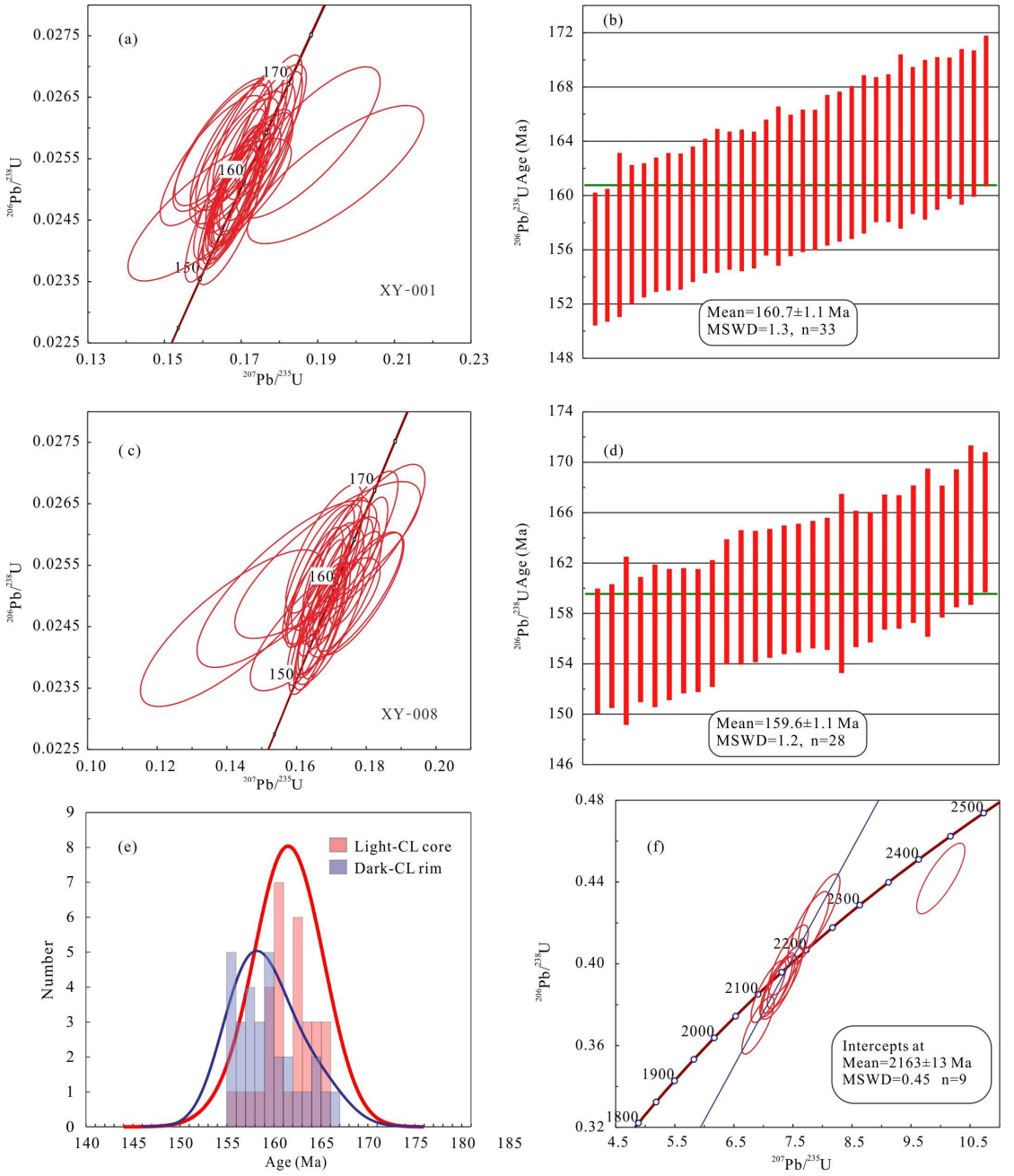

Figure 7. Concordia diagrams for zircon LA-ICP-MS U-Pb analyses.

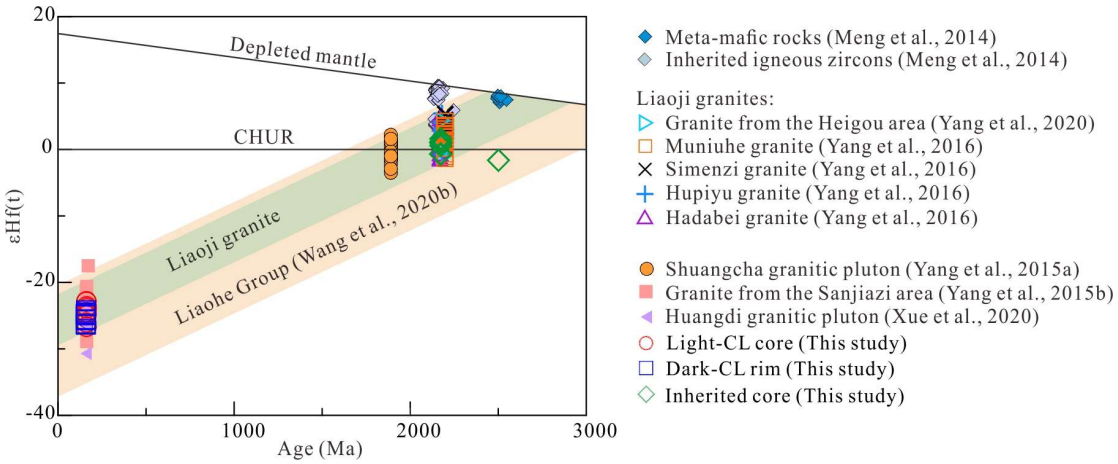

Figure 8. Zircon εHf(t)-age (Ma) diagram for samples in this study and published data for the region.

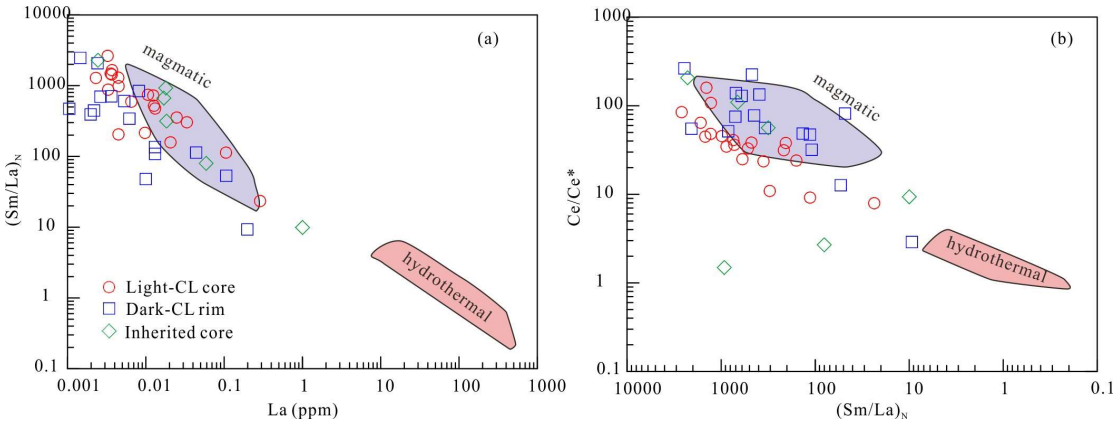

Fig. 9. Discrimination plots for magmatic and hydrothermal zircon (Hoskin, 2005).

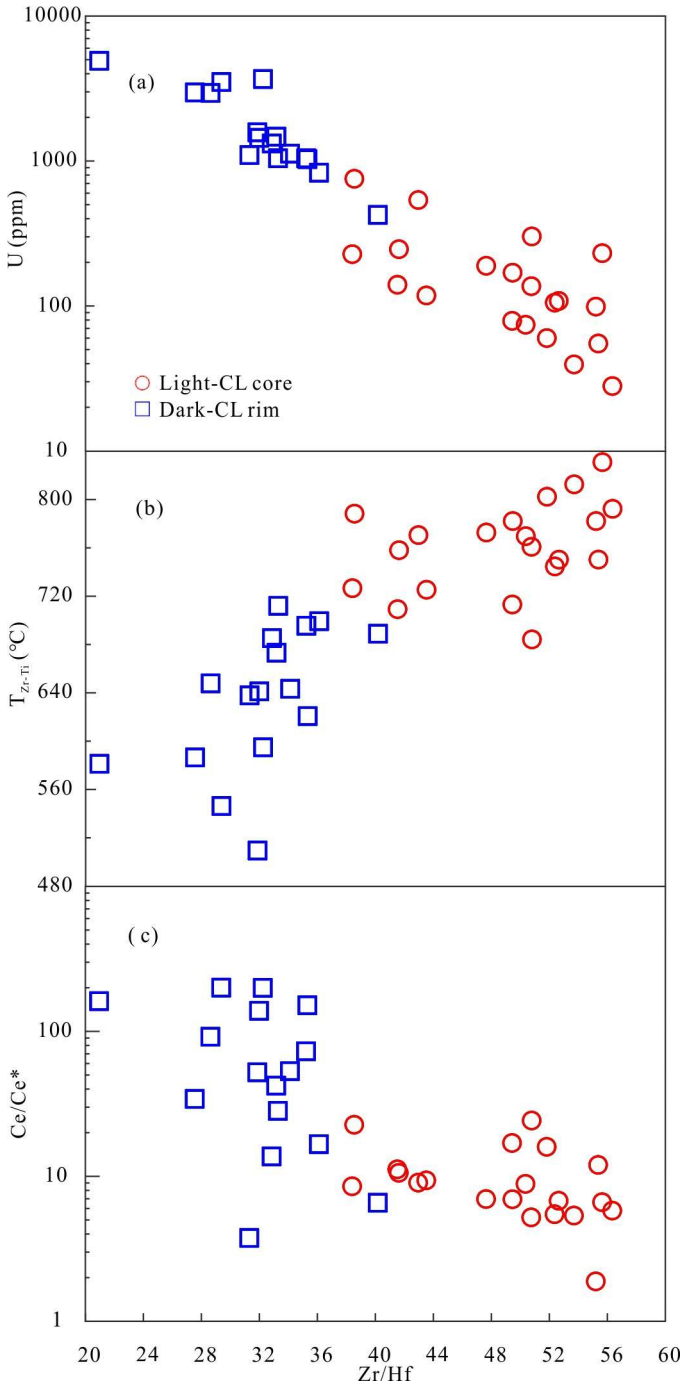

1216

1217 Figure 10. Covariation diagrams for zircon from the Zhoujiapuzi granite. (a) U vs.

1218 Zr/Hf; (b) T_{Zr-Ti} vs. Zr/Hf; (c) Ce/Ce* vs. Zr/Hf.

1219

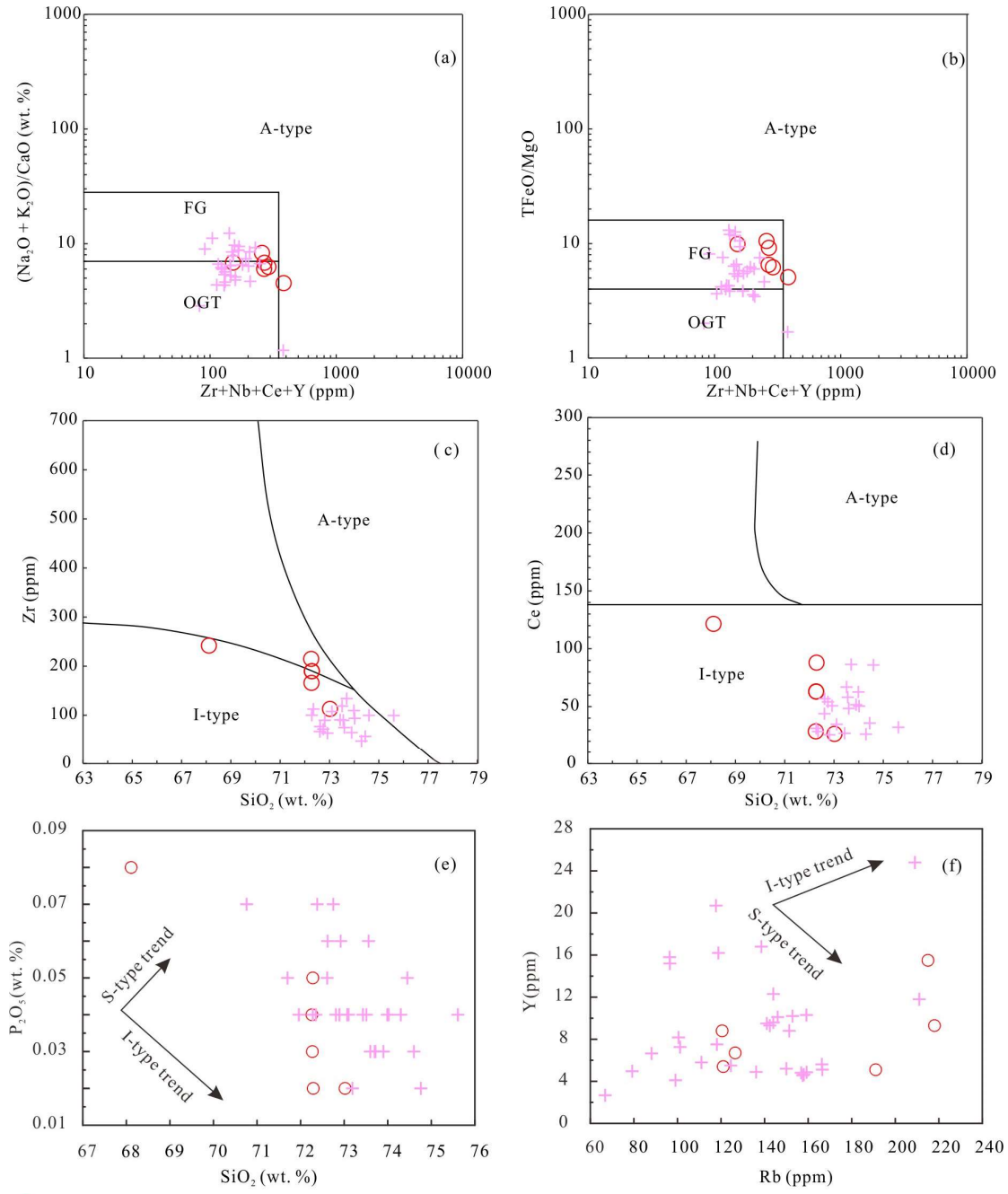

1220

1221 Figure 11. Chemical variation diagrams for the Zhoujiapuzi granite. (a and b)

1222 Zr+Nb+Ce+Y vs. $(Na_2O + K_2O)/CaO$ and TFeO/MgO (after Whalen et al., 1987); (c

1223 and d) SiO_2 vs. Zr and Ce (after Collins et al., 1982); (e) SiO_2 vs. P_2O_5 diagram; (f)

1224 Rb vs. Y diagram

1225

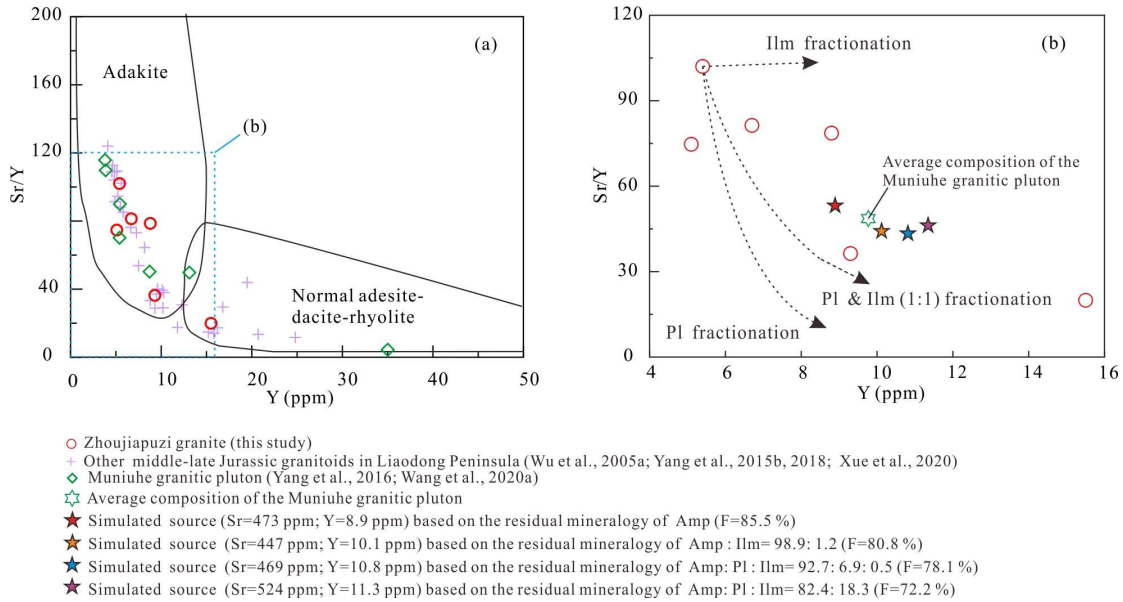

1226

1227 Figure 12. Adakite discrimination diagrams for the Zhoujiapuzi granite (after Defant

1228 and Drummond, 1990).

1229

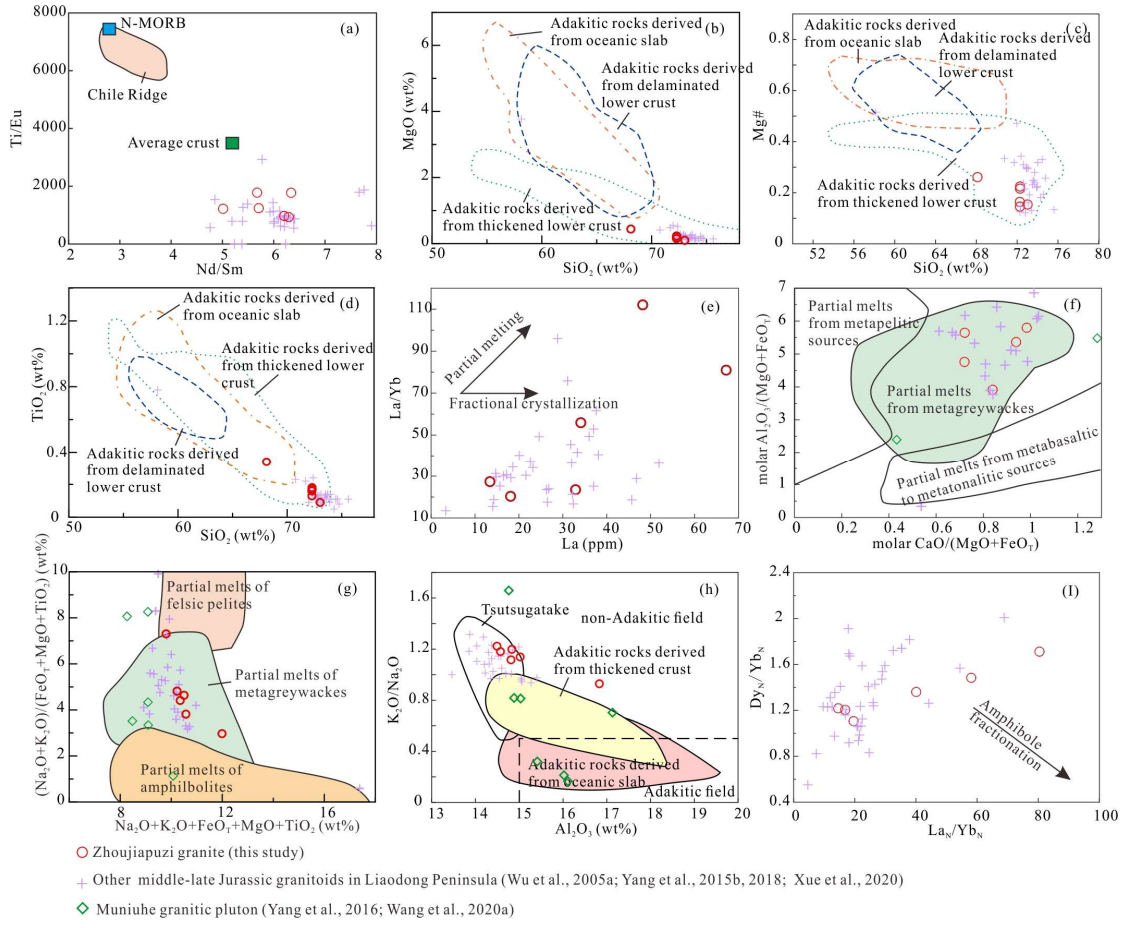

1230

1231 Figure 13. Source characteristics (a-d and f-h) and crystal fractionation (e and i)

discrimination diagrams for the Zhoujiapuzi granite. Plots of (a) Nd/Sm vs. Ti/Eu (Yu et al., 2012); (b-d) SiO_2 vs. MgO, Mg# and TiO_2 (after Wang et al., 2006); (e) La vs. La/Yb (Gao et al., 2007); (f) molar $Al_2O_3/(MgO+FeO_T)$ vs. molar $CaO/(MgO+FeO_T)$ (after Altherr et al., 2000); (g) $(Na_2O+K_2O)/(FeO_T+MgO+TiO_2)$ vs. $Na_2O+K_2O+FeO_T+MgO+TiO_2$ (after Patiño Douce, 1999); (h) K_2O/Na_2O vs. Al_2O_3 diagrams (after Kamei et al., 2009); (i) La_N/Yb_N vs. Dy_N/Yb_N.

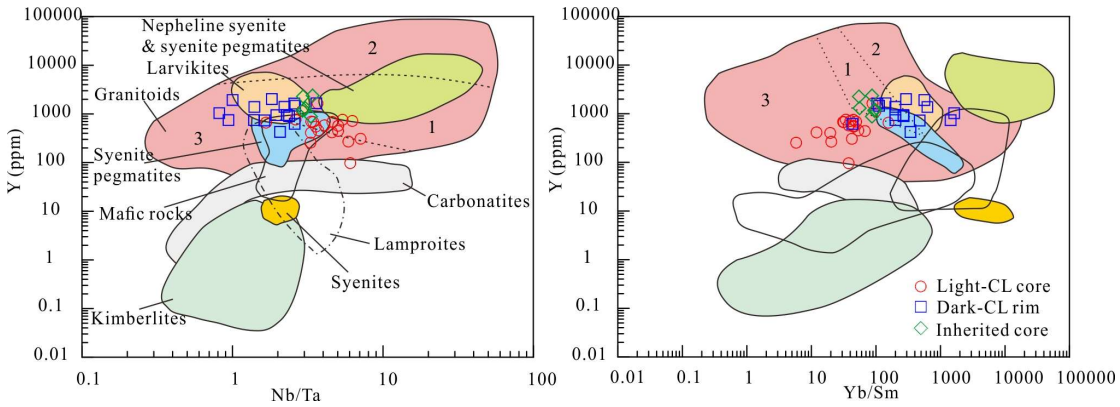

Figure 14. The fields of zircon compositions used as discriminants for different rock types (after Belousova et al., 2002). 'Granitoids' include: 1 aplites and leucogranites; 2 granites; 3 granodiorites and tonalities